Available online at www.sciencedirect.com
SCIENCE DIRECT®
Journal of Organometallic Chemistry 690 (2005) 5215–5236
Journal of Organometallic Chemistry
www.elsevier.com/locate/jorganchem

Mechanistic investigation of the thermal decomposition of Biphen(OP*i*-Pr)$PtEt_2$: An entrance into C–C single bond activation?

Klaus Ruhland *, Eberhardt Herdtweck

TU München, Department Chemie, Lehrstuhl für Anorganische Chemie, Lichtenbergstr. 4, D-85748 Garching, Germany

Received 29 January 2005; received in revised form 7 April 2005; accepted 7 April 2005
Available online 15 June 2005

Abstract

Biphen(OP*i*-Pr) and (COD)$PtCl_2$ give Biphen(OP*i*-Pr)$PtCl_2$ which upon treating with ethyl Grignard forms Biphen(OP-*i*-Pr)$PtEt_2$. The thermal decomposition of Biphen(OP*i*-Pr)$PtEt_2$ was investigated in the temperature range of 353–383 K. The clean and quantitative formation of the Pt(Ethene) adduct was observed. X-ray structures of a molecule in the solid state of all three reaction products and two further related complexes with phenyl fingers instead of *i*-Pr have been determined. For the complexes with *i*-Pr fingers a decisive deviation from a square plane is observed in contrast to the complexes with phenyl fingers. The P–Pt–P angle increases from about 95° in Biphen(OP*i*-Pr)$PtCl_2$ to about 120° in Biphen(OP*i*-Pr)Pt(Ethene), forcing the bridging C–C single bond of the biphenyl fragment as near as 4.17 Å to the Pt center. No through-space coupling between the bridging C atoms and the Pt center could be observed in ^{13}C NMR spectroscopy. No bond lengthening of the bridging C–C single bond in the biphenyl fragment was observed in Biphen(OP*i*-Pr)Pt(Ethene) in comparison to the precursor complexes. The thermal decomposition of Biphen(OP-*i*-Pr)$PtEt_2$ can be described by a first-order kinetic and the activation parameters were determined (temperature range: 353–383 K; $\Delta H^{\ddagger} = 173.8 \pm 16.2$ kJ/mol and $\Delta S^{\ddagger} = 104.7 \pm 44.1$ J/(mol K)). The reaction kinetics were also measured for perdeuterated ethyl groups yielding in a kinetic isotopic effect of 1.56 ± 0.14 which was almost temperature-independent. Selective deuteration at α and β position of the ethyl group, respectively, showed that β-H elimination takes place fast in comparison to the complete thermolysis. In the temperature range of 333–353 K only a scrambling of the deuterium atoms was found without further decomposition (temperature range: 333–353 K; $\Delta_{scram} H^{\ddagger} = 76.1 \pm 15.2$ kJ/mol, $\Delta_{scram} S^{\ddagger} = -80.7 \pm 45.5$ J/(mol K) for Biphen(OP*i*-Pr)$PtEt_2$-d^6). The ethene is not lost during the scrambling process. The scrambling process is connected with a primary KIE decisively larger than 1.56. Biphen(OP*i*-Pr)Pt(Ethene) exchanges the coordinated ethene with ethene in solution as proven by labeling experiments. Both a dissociative and an associative mechanism could be shown to take place as ethene exchange reaction by means of VT ^1H NMR spectroscopy via line shape analysis (temperature range: 333–373 K; $\Delta_{ass} H^{\ddagger} = 26.9 \pm 29.6$ kJ/mol, $\Delta_{ass} S^{\ddagger} = -148.0 \pm 87.5$ J/(mol K), $\Delta_{diss} H^{\ddagger} = 86.0 \pm 6.5$ kJ/mol, $\Delta_{diss} S^{\ddagger} = 5.4 \pm 17.8$ J/(mol K)). The Pt(0) complex formed during the dissociative loss of ethene activates several substrates among them: O_2, H_2, H_2SiPh_2 via Si–H activation, MeI presumably via forming a cationic methyl adduct and ethane via C–H activation but it was proven that the bridging C–C single bond of the biphenyl fragment is not even temporarily broken. The materials were characterized by means of ^1H NMR, ^{13}C NMR, ^{31}P NMR, ^{195}Pt NMR, EA, MS, IR, X-ray analysis and polarimetric measurement where necessary.

Keywords: Pt complexes; Reaction mechanism; C–C activation; Kinetic isotope effect

1. Introduction

Despite of the growing interest in it [1], the controlled activation and cleavage of C–C single bonds by transition metal complexes is still one of the most challenging

* Corresponding author. Tel.: +49 89 289 13096; fax: +49 89 289 13473.
E-mail address: klaus.ruhland@ch.tum.de (K. Ruhland).

0022-328X/$ - see front matter © 2005 Elsevier B.V. All rights reserved.
doi:10.1016/j.jorganchem.2005.04.048

and yet least well understood reactions in chemistry. The challenging character originates from the usually low thermodynamic stability of metal carbon bonds and the kinetic inertness (orbital reorientation during the cleavage) and steric protection (substituents on the carbon atoms) of C–C single bonds. In many of these respects especially the bridging C–C single bond in biphenyl fragments provides promising perspectives: metal–C(sp^2) bonds (formed in the process of activation) are thermodynamically more stable than M–C(sp^3) bonds [2]. The two sp^2-carbons are sterically easier available than sp^3-carbons and the orbital reorientation energy is expected to be lower because of the participation of the phenyl p-orbitals which are ideally directed toward the metal center. Moreover, decomposition reactions, as for instance β-H elimination, after a potential activation are not likely to occur in biphenyl fragments. Remembering the great success of C–C coupling reactions yielding in biphenyls catalyzed in general by group 10 metals and also remembering the principle of microscopic reversibility the cleavage of the bridging C–C single bond in a biphenyl fragment must for sure be kinetically allowed. Taking all this into account, it must come as a surprise that reports into this area are rare and disappointing. The intermolecular reaction was only performed successfully using the highly strained biphenylene (Scheme 1) [3].

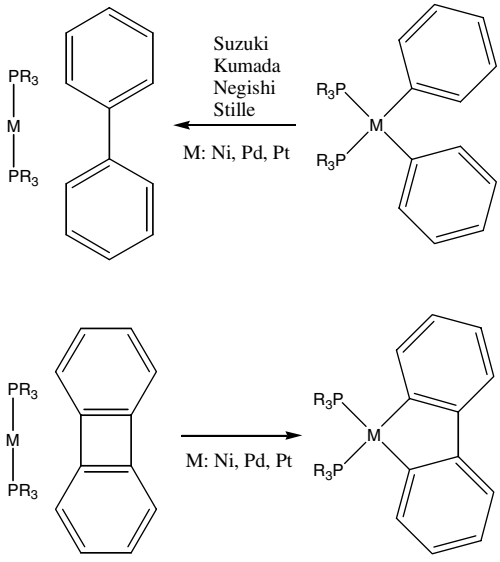

Scheme 1.

No reports about a successful activation of the bridging C–C single bond in non-strained biphenyl fragments went into our attention, yet. The most prominent and promising strategy to enable the activation of non-strained C–C single bonds is to do it intramolecularely by chelating assistance [4], forcing and fixing the C–C single bond under focus statically near to the metal center and generating in general a favorable five-membered ring in case of a cleavage of that bond. One of the most successful examples of this strategy is that of Milstein and co-workers [4e–h] using a pincer ligand. But even with these additional aspects no bridging C–C single bond in a non-strained biphenyl fragment could yet be cleaved to our knowledge. Our idea to enhance the chance for a C–C single bond activation was to not only statically bring the C–C single bond near to the metal by chelating assistance but by additionally inducing an impulse of motion along the potential reaction coordinate for the activation through the experimental settings (Scheme 2). We decided to use the thermolysis of Pt diethyl complexes for this purpose.

The strategy may be visualized by a "shouting an arrow" picture. The arrow in this picture is either the diethyl fragment in (**1**) or the coordinated ethene in (**4**) in Scheme 2. The chord of the bow is the chelating

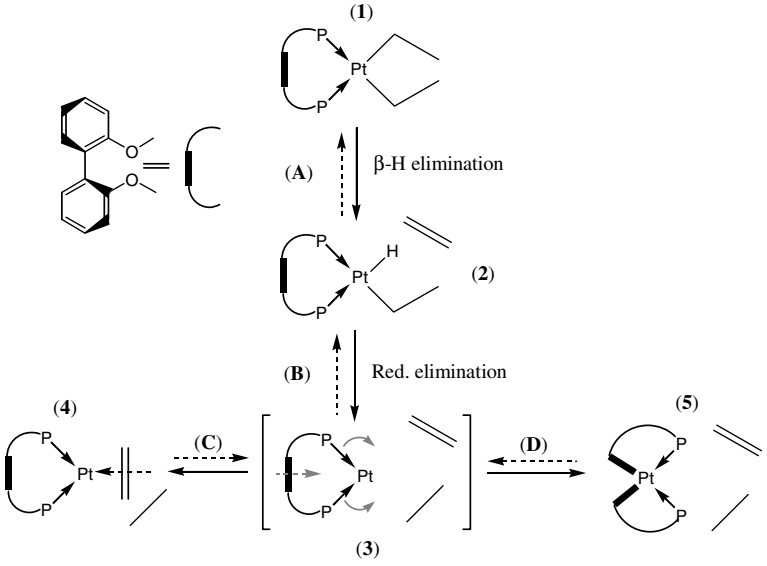

Scheme 2.

ligand. Thus, by removing the diethyl fragment (via β-H elimination and reductive elimination) or the ethene (via dissociation) – i.e., by shouting the arrow- the starting Pt-complex suddenly finds itself in a situation of a Pt(0) center with coordination number two striving for a linear overall coordination geometry. This "relaxation of the bow" induces the impulse of motion along the potential reaction coordinate and offers an additional driving force for a C–C single bond cleavage or activation. As linker between the biphenyl fragment and the coordinating phosphorus "hands" we chose an oxo-group because C–O as well as the O–P represent the shortest bond lengths we could think of as bridging unit and, thus, would force the C–C-single bond under focus as close as possible to the metal center.

2. Results and discussion

2.1. Ligand synthesis and complexation

The ligands that contain the biphenyl fragment were synthesized according to Scheme 3.

For ligand [**3**] with phenyl "fingers" on the phosphorus hand the synthesis is best performed in diethylether with triethylamine as base and at room temperature. For the ligands [**1**], [**2**] and [**4**] with less electrophilic dialkyl "fingers" the synthesis is done in the more polar acetonitrile and at 60 °C to obtain good yields. Ligands [**2**] and [**3**] are both white solids and fairly stable to air ([**3**] being more stable than [**2**]). Longer storage should be done under inert gas atmosphere, though. Ligand [**1**] is a colorless oil that forms macro-crystals at room temperature over weeks and must be rigorously stored under inert gas to prevent oxidation of the phosphorus. The signals in ^{31}P NMR for ligands [**1**], [**2**] and [**4**] show up at about 146 ppm; for ligand [**3**] the signal is found at 113 ppm. The *cis*-[ligand]$PtCl_2$ complexes were received by ligand exchange reaction between (COD)$PtCl_2$ and the ligand in CH_2Cl_2 at room temperature in good yields (Scheme 4). It was checked by mass spectroscopy that oligomerization or polymerization via intermolecular reaction is not a concern in this reaction even if it is worked at high concentration.

All complexes show C_2 symmetry in NMR spectroscopy, though, as will be shown below in the solid state most of the complexes are found to be C_1 symmetric. The two phosphorus atoms are equivalent and the coupling constant $^1J_{PPt}$ to ^{195}Pt is about 4150 Hz proving the *cis* configuration at the metal center [5]. After

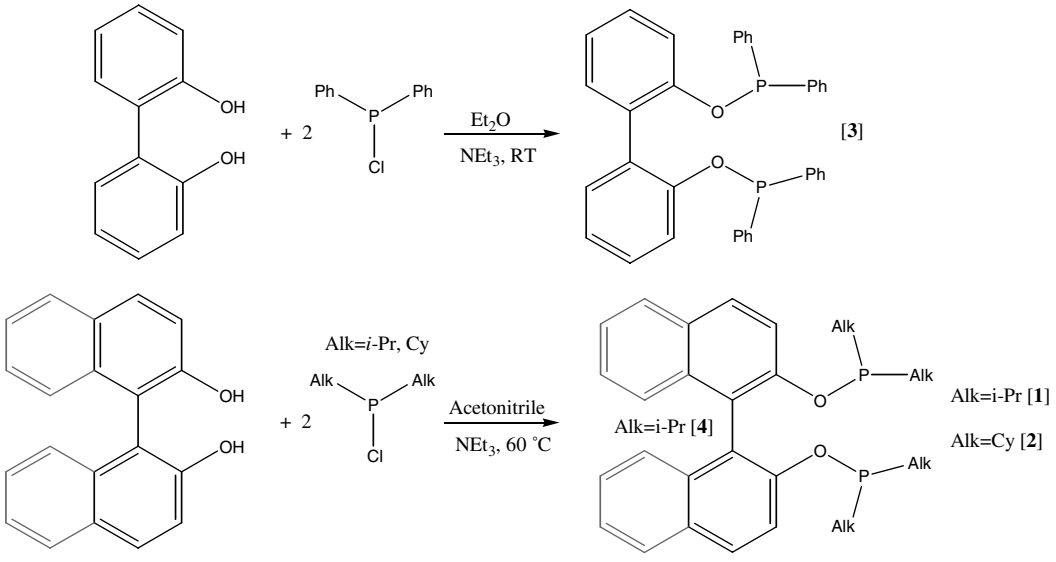

Scheme 3.

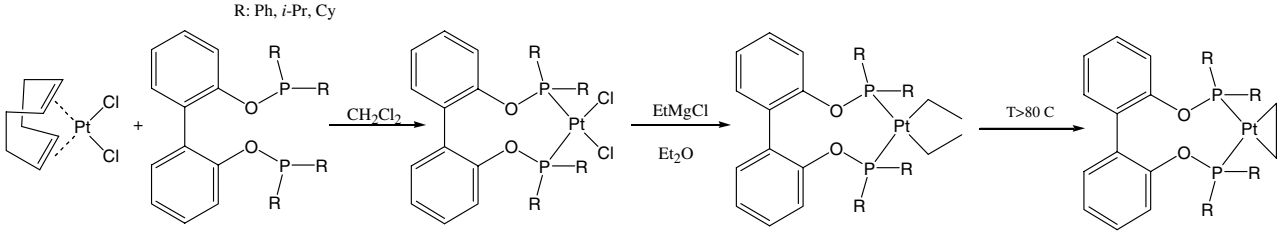

Scheme 4.

treatment of *cis*-[ligand]$PtCl_2$ with two equivalents of EtMgBr in diethylether the *cis*-[ligand]$PtEt_2$ complex is received for all ligands in acceptable yields (Scheme 4).

2.2. Structural and spectroscopic comparison of the complexes employed

If [**1**]$PtEt_2$ is heated to temperatures higher than 356 K in toluene-d^8 a clean decomposition reaction yielding into [**1**]Pt(Ethene) starts (Schemes 4 and 5). This behavior is known for related complexes [6]. Via ^1H NMR spectroscopy, the evolution of ethane can be detected as a singulet at 0.76 ppm. Also, traces of free ethene show up after some time as a singulet at 5.25 ppm. The ^{31}P NMR shows the disappearance of a peak at 160 ppm with a coupling constant $^1J_{PPt} = 1971$ Hz belonging to the starting material in favor of a new peak at 186 ppm with a coupling constant $^1J_{PPt} = 4060$ Hz for [**1**]Pt(Ethene) (Scheme 5).

The reaction yields quantitatively into the product peak at 186 ppm. In some cases the reaction solution turns darker with the reaction time, but neither ^1H NMR nor ^{31}P NMR spectroscopy give hints for significant amounts of any decomposition products. [**1**]Pt(Ethene) can be isolated by removing the toluene in vacuo and crystallized from hexane. An X-ray structure of a molecule in the solid state could be received which is shown in Scheme 6 in comparison with X-ray structures of [**1**]$PtCl_2$, [**3**]$PtCl_2$, [**3**]$PtEt_2$ and [**1**]$PtEt_2$ shown as ORTEP style plot of the compound in the solid. Thermal ellipsoids are drawn at the 30% probability level. Hydrogen atoms are omitted for clarity.

Table 1 and Scheme 6 show that a decisive structural change takes place during the course of the synthesis with [**1**] according to Scheme 4. The P–Pt–P angle increases from about 95° in [**1**]$PtCl_2$ to 110° in [**1**]$PtEt_2$ up to 120° in [**1**]Pt(Ethene). The distortion of the pseudo-square plane becomes larger forcing the bridging C–C single bond of the biphenyl fragment nearer to the Pt center, as was planned in the basic strategy. The three X-ray structures of [**1**]$PtCl_2$, [**1**]$PtEt_2$ and [**1**]Pt(Ethene) can – concerning the biphenyl fragment – be regarded as spot shots of the trajectory along the C–C activation pathway. Table 1 and Scheme 6 also show that for [**3**]$PtCl_2$ and [**3**]$PtEt_2$ the distortion away from the pseudo-square planar geometry is much less pronounced. It will be shown later in this paper that there is also a great difference in the behavior of the two complexes ([**1**]$PtEt_2$ and [**3**]$PtEt_2$) concerning the thermal decomposition.

DFT calculations in GAUSSIAN-03 [7] for [**1**]Pt(Ethene) using different functionals (B3LYP, B3PW91) and different basis sets (LANL2DZ, 6-311g(d,p) for C H O P and Stuttgart ECP60MDF [8] for Pt) did not reproduce the large P–Pt–P angle found by X-ray analysis for [**1**]Pt(Ethene) (Table 2). For [**1**]$PtEt_2$, the P–Pt–P is also calculated decisively too small, while in the case of [**3**]$PtEt_2$ the structure calculation is satisfactory even on the B3LYP/LANL2DZ level. We conclude from this that the structure of [**3**]$PtEt_2$ is dominated by electronic

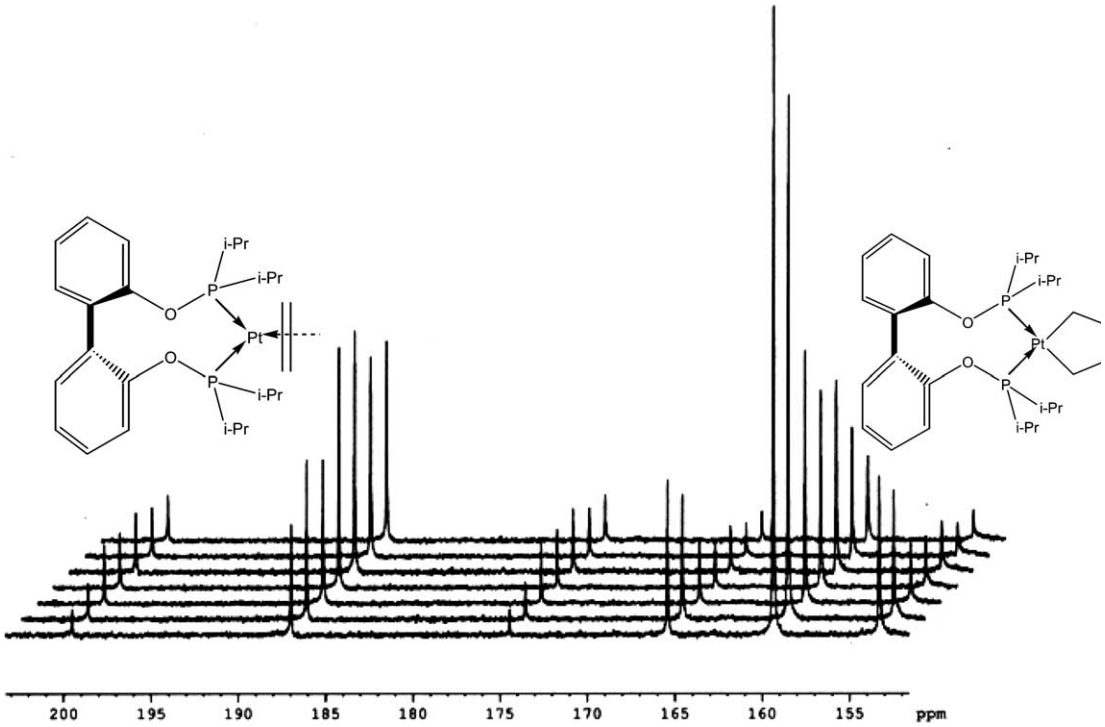

Scheme 5.

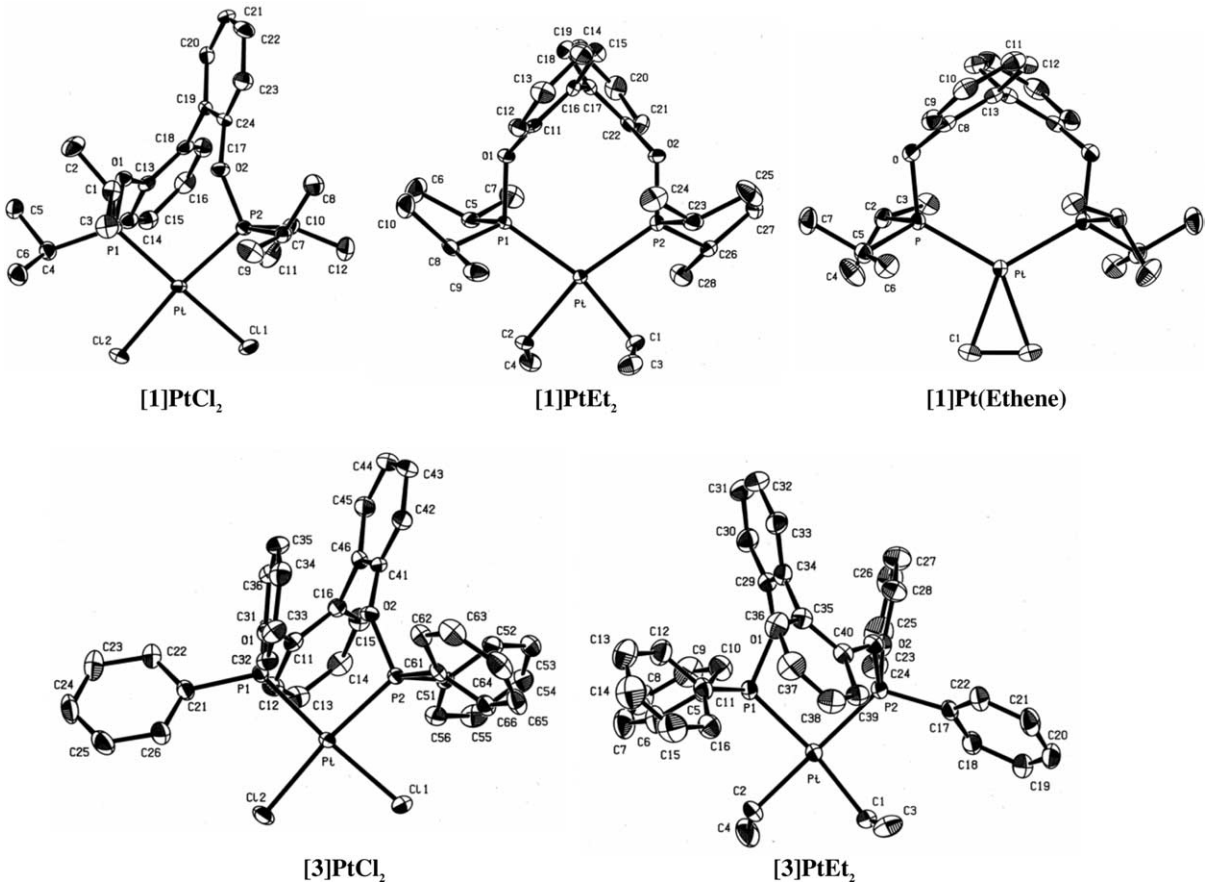

Scheme 6.

Table 1
Comparison of the most indicative structural parameters determined by X-ray analysis

	[3]$PtCl_2$	[3]$PtEt_2$	[1]$PtCl_2$	[1]$PtEt_2$	[1]Pt(Ethene)
Pt–P1 (Å)	2.2305(6)	2.2492(7)	2.2321(12)	2.2671(8)	2.2470(4)
Pt–P2 (Å)	2.2200(8)	2.2653(7)	2.2291(11)	2.2702(9)	2.2470(4)
Pt–X1 (Å)	2.3532(6)	2.128(3)	2.3671(12)	2.126(4)	2.1194(19)
Pt–X2 (Å)	2.3490(8)	2.114(3)	2.3534(12)	2.135(3)	2.1194(19)
C_a–C_b (bridging) (Å)	1.482(4)	1.491(4)	1.483(7)	1.493(5)	1.488(2)
Pt···C_a (bridging) (Å)	4.824(3)	4.875(3)	4.391(4)	4.670(3)	4.170(2)
Pt···C_b (bridging) (Å)	4.247(3)	4.304(3)	4.896(4)	4.676(3)	4.170(2)
P–Pt–P (°)	91.92(3)	91.81(3)	95.52(4)	109.08(3)	120.27(2)
X–Pt–X (°)	89.05(3)	84.40(11)	89.12(4)	81.45(13)	39.25(8)

Crystallographic data are given in Table 6 at the end of the paper.

Table 2
Calculated structure parameters of [1]Pt(Ethene) and the X-ray data for comparison

	X-ray	B3LYP/LANL2DZ	B3LYP/6-311g(d,p)[a]	B3PW91/6-311g(d,p)[a]
Pt–P (Å)	2.247	2.404	2.315	2.287
Pt–C (Å)	2.119	2.134	2.140	2.120
C═C (Ethene) (Å)	1.424	1.458	1.435	1.437
P–Pt–P (°)	120.3	99.7	103.2	103.3
C–Pt–C (°)	39.3	39.9	39.2	39.6

[a] For Pt the Stuttgart, ECP60MDF basis set was used [8].

factors while that of [**1**]$PtEt_2$ and [**1**]Pt(Ethene) is dominated by sterics. The structure of the [ligand]$PtCl_2$ complex seems to be dominated by electronic effects in both cases [**1**]$PtCl_2$ and [**3**]$PtCl_2$. We propose that this is because in the latter case the decline in the *trans* influence along the P–Pt–X axis is most pronounced and, thus, leads to the strongest electronic stabilization if the square planar geometry is realized through synergistic electronic push/pull effect.

X-ray structures of a molecule in the solid have been reported for $(PPh_3)_2$Pt(Ethene) [9a] and $(PCy_3)_2$Pt(Ethene) [9b]. While the C=C bond length of coordinated ethene (1.424 Å in [**1**]Pt(Ethene) was found to be longer in both complexes (1.434 and 1.440 Å) the P–Pt–P angle was reported to be decisively smaller (111.6° and 116.3°).

Considering the X-ray analysis data, one would think [**1**]Pt(Ethene) is best described as a Pt(II) center within a metallacyclopropane because of the pseudo-square planar structure found. The spectroscopic data tell a different story, though. In ^{13}C NMR spectroscopy, the coordinated ethene shows up at about 16 ppm as broad pseudo-triplet. No coupling to ^{31}P can be resolved in contrast to the Pt–CH_2 carbon atom in [**1**]$PtEt_2$ which shows the expected doublet of doublets of a pseudo-triplet in ^{13}C NMR spectroscopy (Fig. 1). The carbon atoms in [**1**]Pt(Ethene) behave (concerning coupling and chemical shift in ^{13}C NMR spectroscopy) similar to the $PtCH_2$–CH_3 indicating that on the time scale of ^{13}C NMR spectroscopy the coordinated ethene is freely rotating and, thus, [**1**]Pt(Ethene) is better described as a Pt(0) complex with coordinated ethene. The rotational behavior of ethene, coordinated to Pt(0) has been studied before [10].

Also, the $^1J_{PPt}$ is not in accordance with the assumption of a Pt(II)–metallacyclopropane. This coupling constant is a function mainly of the ligand *trans* to the P atom, the bond length P–Pt and – in chelating ligands with two P donors – of the bond angle P–Pt–P [5]. In our case the $^1J_{PPt}$ is dominated almost completely by the *trans*-ligand which itself, of course, influences the P–Pt bond length. Switching from [**1**]$PtCl_2$ with $^1J_{PPt}$ = 4147.2 Hz to [**1**]$PtEt_2$ the $^1J_{PPt}$ drops to 1971.4 Hz as a consequence of the much stronger *trans* influence of an alkyl group in comparison to Cl. In [**1**]Pt(Ethene), however, $^1J_{PPt}$ is found to be 4060.7 Hz which is not in accordance with the assumption of two alkyl ligands *trans* to the P atoms and, thus, in contradiction to a metallacyclopropane description.

The chemical shift in ^{195}Pt NMR spectroscopy, unfortunately, does not allow to distinguish between Pt(II) and Pt(0) unequivocally [5d]. A key question for the success of the proposed strategy is: Does the Pt center know about the existence of the bridging C atoms in the biphenyl fragment about 4.17 Å away and can we prove that? One criterion would be a bond lengthening of the bridging C–C single bond in the biphenyl fragment, but as Table 1 shows, this is unequivocally not observed. Another possibility is to watch out for a through-space coupling between the ^{195}Pt center and the ^{13}C nuclei of the bridging carbon atoms in the biphenyl fragment potentially visible in ^{13}C NMR spectroscopy (a $^4J_{CPt}$ through-bond coupling is too small to be detected). That through-space coupling between Pt and C atoms does play a role, can be seen in Fig. 1. We assume that the large J_{CPt} coupling of the three methyl groups on the far left in Fig. 1 which in [**1**]$PtCl_2$ is not present (they show up as singulets each), are at least partly due to a through-space coupling, clearly visible in [**1**]$PtEt_2$ and [**1**]Pt(Ethene). These methyl groups are

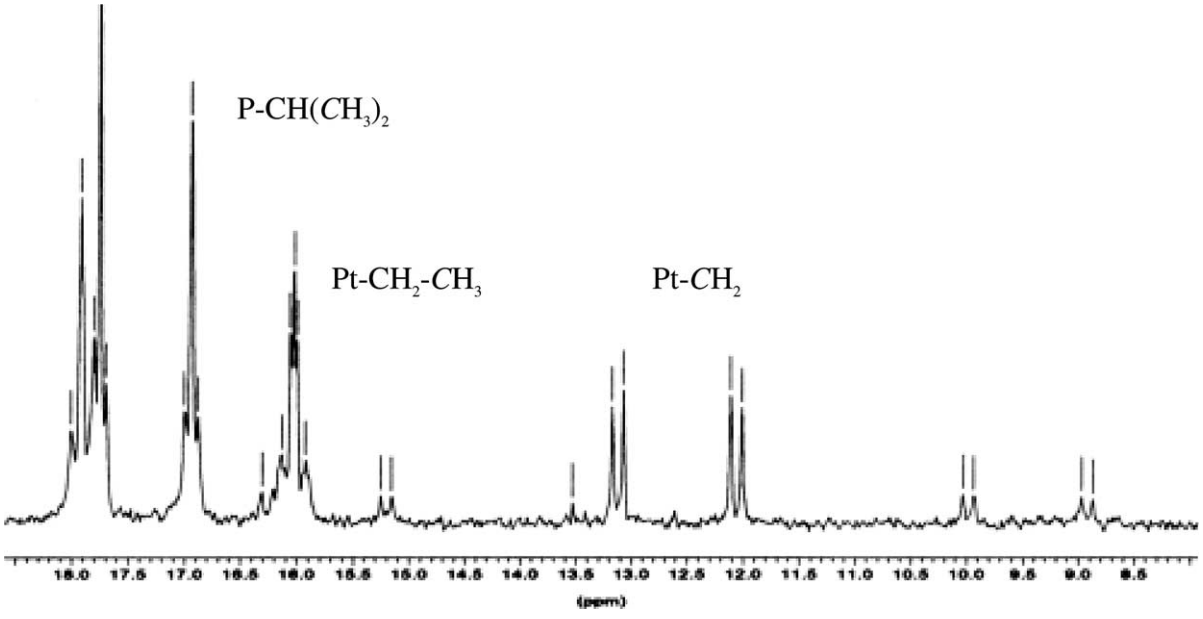

Fig. 1. Aliphatic area of the ^{13}C NMR spectrum of [**1**]$PtEt_2$ in toluene-d^8.

about 3.5 Å away from the Pt center. However, it was carefully checked for [**1**]Pt(Ethene) and [**4**]Pt(Ethene) that unequivocally no through-space coupling between the ^{195}Pt center and the bridging C atoms of the biphenyl fragment is detectable (the location of the signals for the bridging carbon atom in the ^{13}C NMR spectrum was confirmed through measurement without broad band decoupling. The bridging carbons show up as singulets under those conditions with a chemical shift that unequivocally allows to distinguish them from the second quarternary carbon atom in the molecule bound to oxygen.) Thus, in the starting complex [**1**]Pt(Ethene) (the "drawn bow") there is, unfortunately, no evidence that the two reaction partners (the Pt center and the bridging C–C single bond in the biphenyl fragment) know of each other.

2.3. Mechanistic investigation of the thermal decomposition

The thermal decomposition of [**1**]$PtEt_2$ was successfully described by first-order kinetics in [**1**]$PtEt_2$ shown in Fig. 2 for two concentrations at 363 K.

The kinetics were investigated for several temperatures in the range of 353–378 K to determine the activation parameters. An evaluation of the data via Eyring plot yields in a good correlation to a straight line (Fig. 3).

From this plot the activation parameters for the thermal decomposition of [**1**]$PtEt_2$ were determined to be $\Delta H^{\ddagger} = 173.8 \pm 16.2$ kJ/mol and $\Delta S^{\ddagger} = 104.7 \pm 44.1$ J/(mol K) (errors are given with a confidence radius of 95.4% according to Student's distribution). To get more insight into the mechanism of this reaction the thermal decomposition was also performed for [**1**]$PtEt_2$-d^{10} with perdeuterated ethyl groups. This compound was received analogously to the non-deuterated complex using commercial CD_3CD_2Br as starting material. The peaks for the ethyl group and the coordinated ethene disappear in ^{1}H NMR spectroscopy. In ^{31}P NMR spectroscopy, a slight shift (0.2 ppm) is observed in

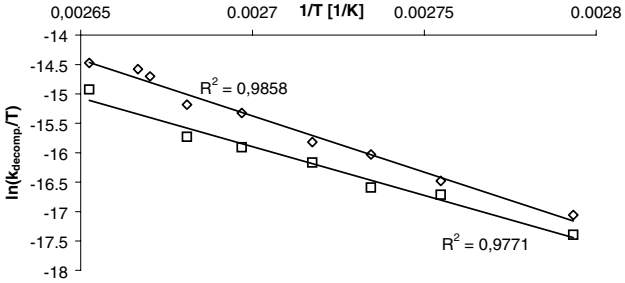

Fig. 3. Eyring plot for the thermal decomposition of [**1**]$PtEt_2$ (□) and [**1**]$PtEt_2$-d^{10} (◇) in toluene-d^8 using the data of Table 3.

comparison to the non-deuterated compound. The IR spectrum shows a shift of several peaks in the area of 2970 cm^{-1} into the region of 2200–2052 cm^{-1} for [**1**]$PtEt_2$-d^{10} and two peaks at 2310 and 2133 cm^{-1} for [**1**]Pt(Ethene-d^4). The result of the Eyring plot for the perdeuterated starting material is seen in Fig. 3. Table 3 shows the quantitative data of the plot in Fig. 3.

As can be seen from Fig. 3, a significant but small kinetic isotopic effect (KIE) H/D of 1.56 ± 0.14 can be established that is almost temperature independent. A value of 1.4 ± 0.1 was reported for the thermolysis of *t*-$(PPh_3)_2Pd(CH_2CD_3)_2$ [11c]. Unfortunately, such small kinetic isotopic effects cannot unequivocally be interpreted without further investigation. A primary kinetic

Table 3
Rate constants for the thermal decomposition of [**1**]$PtEt_2$ and [**1**]$PtEt_2$-d^{10}

T (K)	$k_{H/decomp}$ of [**1**]$PtEt_2$ ($(1/s) \times 10^4$)	$k_{D/decomp}$ of [**1**]$PtEt_2$-d^{10} ($(1/s) \times 10^4$)	k_H/k_D
377	1.955 ± 0.008	1.245 ± 0.01	1.57 ± 0.01
375	1.750 ± 0.008	–	–
374.5	1.545 ± 0.003	–	–
373	0.952 ± 0.005	0.550 ± 0.033	1.73 ± 0.11
370.8	0.822 ± 0.013	0.458 ± 0.015	1.79 ± 0.07
368	0.497 ± 0.008	0.350 ± 0.008	1.42 ± 0.04
365.7	0.400 ± 0.005	0.228 ± 0.008	1.75 ± 0.07
363	0.253 ± 0.013	0.200 ± 0.033	1.27 ± 0.22
358	0.140 ± 0.012	0.100 ± 0.017	1.40 ± 0.26

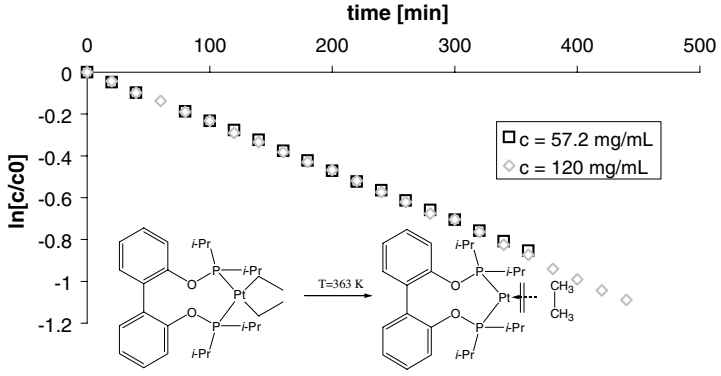

Fig. 2. Evaluation of the thermal decomposition of [**1**]$PtEt_2$ at 363 K described by first-order kinetics at two different concentrations of [**1**]$PtEt_2$ in toluene-d^8.

isotopic effect with small transition angle [12a] or a secondary isotopic effect (especially since the KIE is found to be almost temperature-independent [12b]) can in principle be responsible for the behavior determined. To be able to distinguish between these two cases we examined the partially deuterated complexes [**1**]Pt$(CD_2CH_3)_2$-([**1**]$PtEt_2$-d^4) and [**1**]Pt$(CH_2CD_3)_2$ ([**1**]$PtEt_2$-d^6). *Both* complexes showed KIE H/D of 1.4–1.5 (measurements at 363 K and 373 K). The reason for this contradictive finding is a scrambling of the deuterium atoms via β-H elimination (sub-equilibrium (**A**) in Scheme 2) which is fast in comparison to the complete thermal decomposition. This can unequivocally be monitored by ^{31}P NMR spectroscopy (Scheme 7).

In the temperature range of 323–348 K the scrambling process can be examined as the only reaction taking place. Thermal decomposition cannot be observed in this temperature range before completion of the scrambling. If the scrambling process in [**1**]$PtEt_2$-d^6 is examined under an atmosphere of unlabeled ethene no influence onto the kinetics is found and the final peak pattern in ^{31}P NMR spectroscopy is unchanged to the reaction under argon atmosphere. This proves that the β-H elimination/re-insertion occurs exclusively intramolecularely. The ethene does not leave the coordination sphere during the process. This kind of scrambling behavior has been reported before in a $(PPh_3)_2Pt(Butyl)_2$ complex [11a,b]. For *t*-$(PR_3)_2PdEt_2$ it was reported that no scrambling takes place during the course of thermal decomposition [11c]. If [**1**]$PtEt_2$-d^6 or [**1**]$PtEt_2$-d^4 is heated to 363 K under an atmosphere of unlabeled ethene after less than 30 min the final peak pattern (Scheme 7) is reached in the starting material and remains constant during the further course of the thermal decomposition while for the product [**1**]Pt(Ethene) only one peak for unlabeled coordinated ethene is found in contrast to 3 peaks (one large and two small ones) that are found under argon atmosphere. Thus, exchange of ethene in solution with [**1**]Pt(Ethene) does take place. This will be explained in detail below. Scheme 8 summarizes the knowledge about sub-equilibrium (**A**) of Scheme 2. In both cases ([**1**]$PtEt_2$-d^6 or [**1**]$PtEt_2$-d^4) six isomers are possible via scrambling. Five of them are clearly resolved in the peak pattern shown in Scheme 7.

The scrambling is a three-step process including β-H elimination, rotation of the coodinated ethene and re-insertion. All these processes are, as proven before, intramolecular, and the overall scrambling can be described successfully by a first-order kinetic in [**1**]$PtEt_2$ (with $k_{scram} \approx k_{\beta\text{-H}}$ since the mono-ethyl complex with coordinated ethene cannot be detected). The evaluation was done by subtracting the peak pattern at time *t* from the final distribution pattern and integration of the residing Peak for the starting material (Scheme 7). Quantitative data for [**1**]$PtEt_2$-d^6 is listed in Table 4. An Eyring plot is shown in Fig. 4 yielding in $\Delta H^{\ddagger} = 76.1 \pm 15.2$ kJ/mol and $\Delta S^{\ddagger} = -80.7 \pm 45.5$ J/(mol K) for the overall scrambling process. Later in this paper will be proven that with the scrambling process must be connected a primary KIE much larger than 1.56. This is in accordance with our qualitative observation that [**1**]$PtEt_2$-d^4 scrambles faster than does [**1**]$PtEt_2$-d^6.

These parameters are in accordance with the assumption that the β-H elimination is the rate-determining step

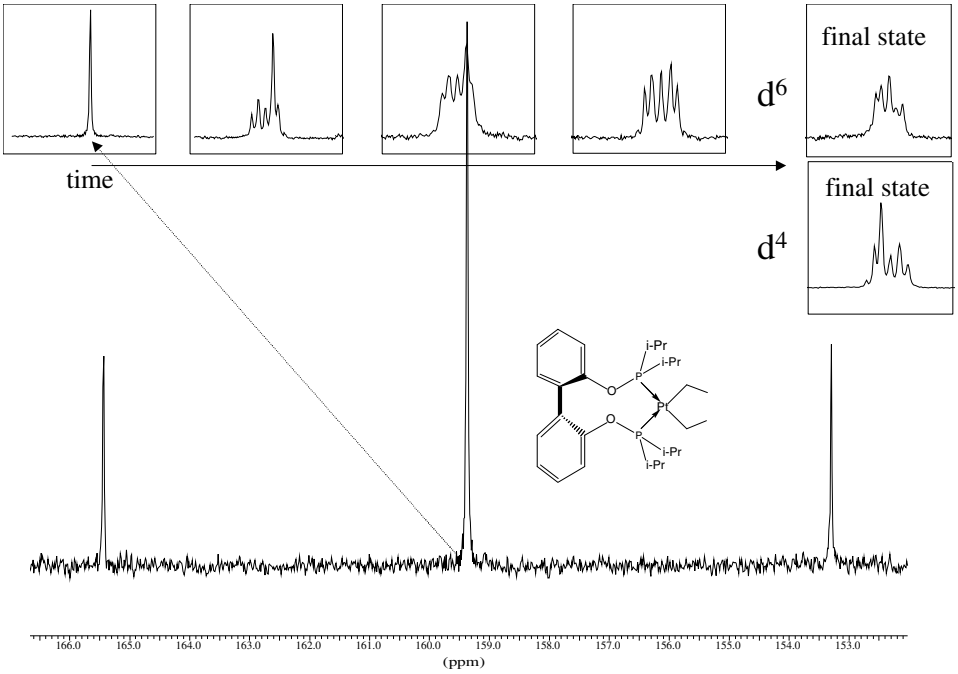

Scheme 7.

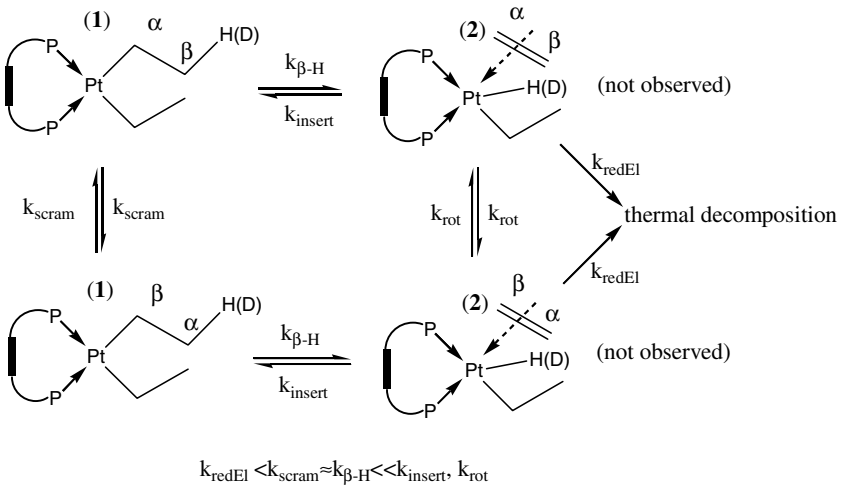

Scheme 8.

Table 4
Rate constants for the deuterium scrambling in [**1**]$PtEt_2$-d^6

T (K)	K_{scram} in [**1**]PtEt-d^6 ($(1/s) \times 10^5$)
338.5	7.92 ± 0.54
331.5	4.38 ± 0.42
327	2.33 ± 0.78
323	1.85 ± 0.51

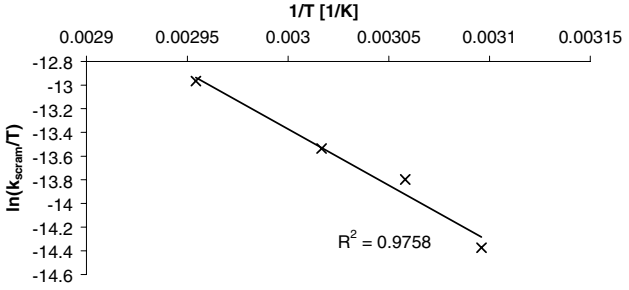

Fig. 4. Eyring plot for the deuterium scrambling in [**1**]$PtEt_2$-d^6 using the data of Table 4.

in the scrambling process (negative $\Delta S^{\ddagger}$ because the free rotation of the ethyl group is decreased).

A mechanism stated for the complete thermal decomposition must explain the almost temperature-independent KIE H/D of 1.56 and the positive activation entropy. Scheme 9 shows the most convincing possibilities.

In pathway (**a**), the KIE is caused through a primary KIE with small transition angle which is expected for an intramolecular reductive elimination. The positive activation entropy is explained because ethane is on its way to leave the molecule. The fact that the product **4** exchanges coordinated ethene with free ethene in solution is not a contradiction to pathway (**a**) as will be shown below. In pathway (**b**), the KIE is explained through a secondary KIE caused through the loss of ethene (change sp^3-like to sp^2 of the ethene's carbons) as rate determining step. A secondary KIE would be in accordance with the almost temperature-independent KIE which is rarely found for primary KIE's [12b]. This step is dissociative and would be in accordance with a

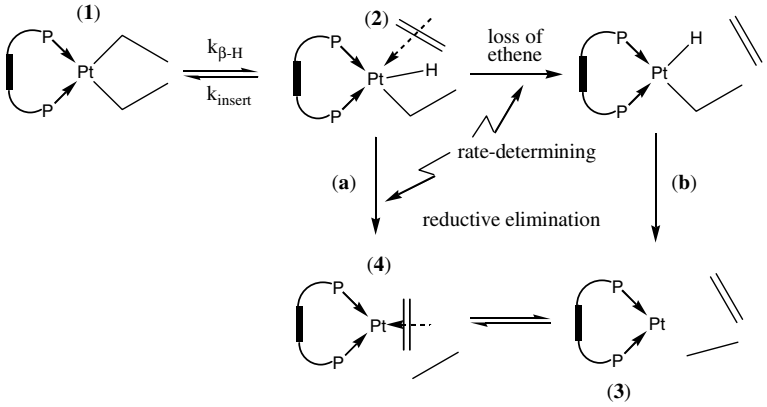

Scheme 9.

positive activation entropy, too. The reductive elimination in pathway (**b**) can be excluded as rate determining step since in that case incorporation of ethene from the solution should have been found. Also if the thermal decomposition is carried out in pyridine-d^5 instead of toluene-d^8 the kinetic behavior does not change significantly. If the rate-determining step was the reductive elimination in pathway (**b**) generating a coordinatively unsaturated compound in the transition state with the ground state being coordinatively saturated, one would have expected an acceleration of the reaction when switching to a coordinating solvent. Performing the thermal decomposition under 133 bar of ethene did not influence the kinetics. From this experiment it can be concluded that an ethene coordination/de-coordination equilibrium is not important for the rate determining step. To influence a potential transition state including the loss of ethene (along pathway (**b**) in Scheme 9), the pressure of ethene must be at least 350 bar to see a reliable effect. This was, unfortunately, out of the range we could examine. Taking all together, our results support pathway (**b**) in Scheme 9 (especially the weak temperature dependence of the KIE is easier to understand then), but we cannot unequivocally distinguish between pathway (**a**) and (**b**). Taking into account the principle of microscopic reversibility pathway (**a**) seems not very likely, since it would mean that ethane attacks directly [**1**]Pt(Ethene) to build [**1**]$PtEt_2$. If [**1**]Pt(Ethene-d^4) is heated to 363 K under an atmosphere of unlabeled ethane over hours the incorporation of (partially) unlabeled coordinated ethene is found. Thus, sub-equilibrium (**B**) of Scheme 2 is reversible (Fig. 5).

Fig. 5 shows that the incorporation of H atoms with the time follows the order $d^4h^0 \rightarrow d^3h^1d^2h^2 \rightarrow d^1h^3 \rightarrow d^0h^4$. From this behavior, we must conclude that the scrambling process must be connected with a large primary KIE, much larger than 1.56. In that case the complete equilibrium shown in Scheme 10 is shifted time after time to the more and more H-atom-containing compounds without forming [**1**]Pt)Ethene-d^0 in the first place.

At this point it must be stated that while [**2**]$PtEt_2$ and [**1**]$PtEt_2$ cannot be distinguished on the base of kinetic measurements of the thermolysis, [**3**]$PtEt_2$ shows a decisively different behavior when heated in toluene to temperatures of about 350 K. If a sample of [**3**]$PtEt_2$ in toluene-d^8 is heated to temperatures of 358 K the only change that is observed in ^1H NMR spectroscopy is that the phenyl fingers begin to rotate in the time scale of the NMR measurement. The signals of the phenyl protons and the signals for the CH_2-group of the ethyl ligands broaden (T_{coal} = 378 K). The signal for the CH_3-group of the ethyl ligands does not change. For an induction period of 1 h nothing else is observed. Then an additional pseudo-triplet at about 145 ppm ($^1J_{PPt}$ = 4132

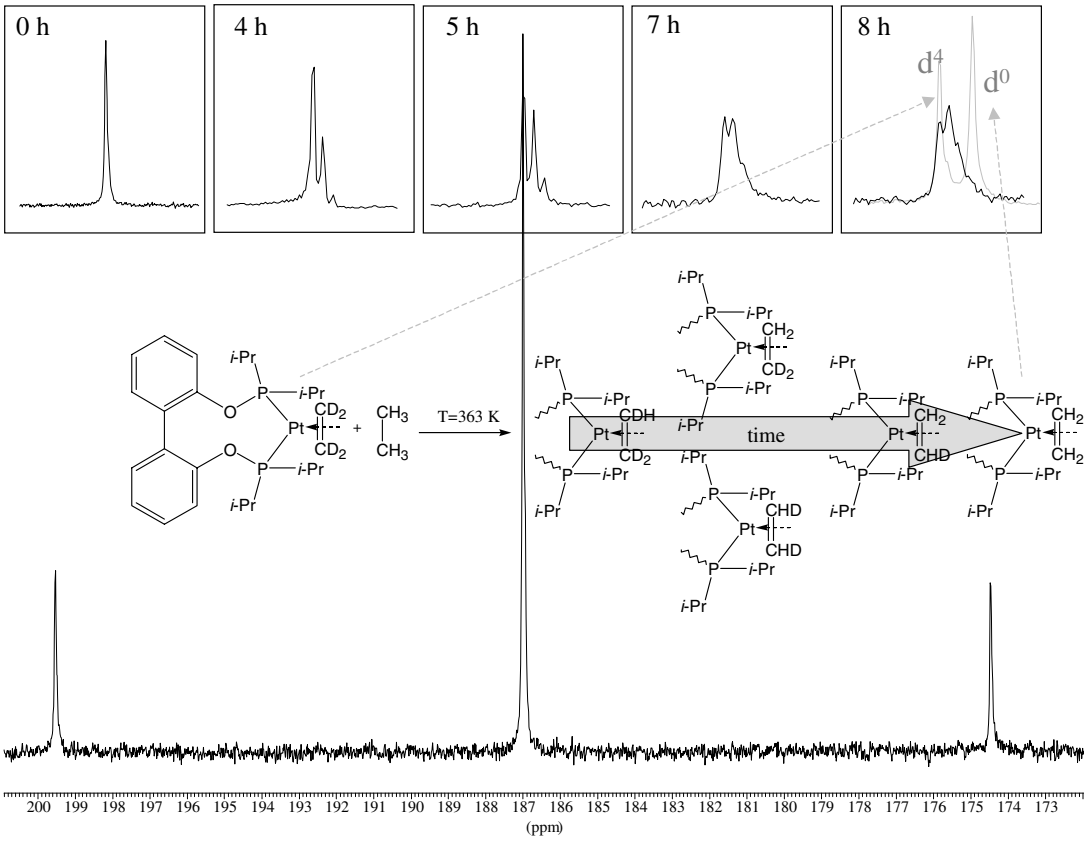

Fig. 5. ^{31}P NMR of [**1**]Pt(Ethene-d^4) that is heated to 363 K under an atmosphere of unlabeled ethane in toluene-d^8.

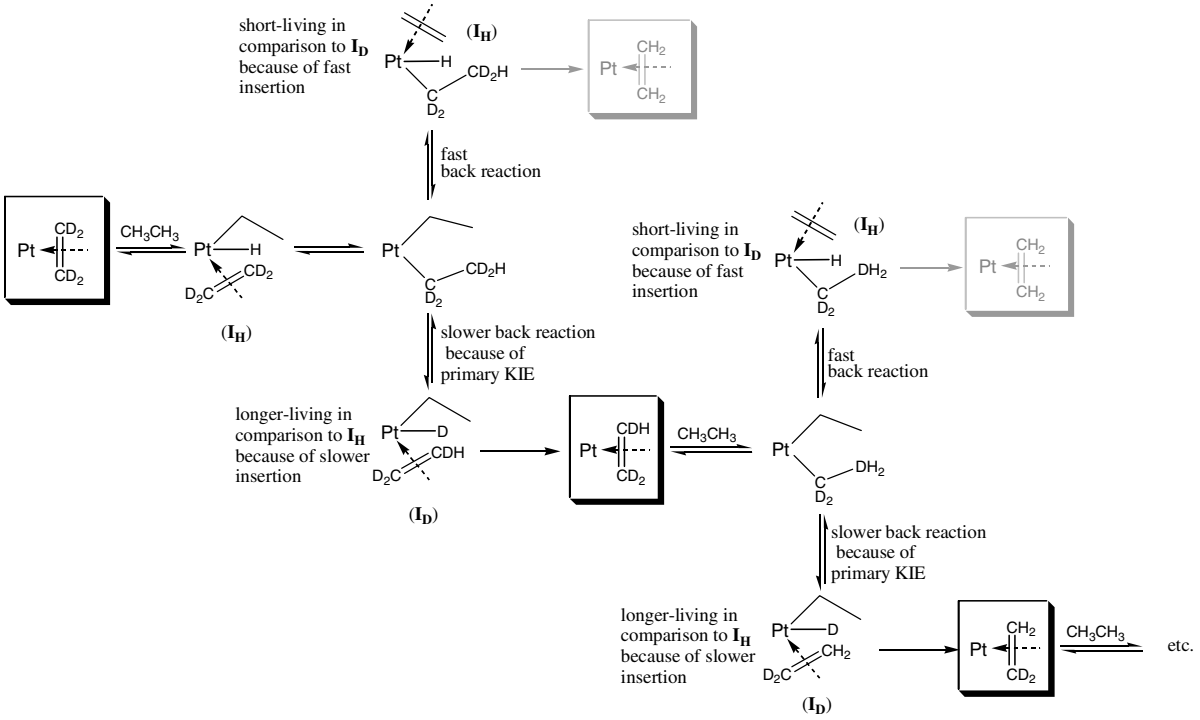

Scheme 10.

Hz) appears in the ^{31}P NMR spectrum and the peaks of the ethyl ligands disappear slowly in the ^{1}H NMR spectrum. Peaks of free ethane and ethene show up. However, the reaction does not go cleanly to completion and it must be concluded that the new product (most likely [**3**]Pt(Ethene)) is not stable. This behavior is not yet well understood.

As was mentioned the product of the thermal decomposition, [**1**]Pt(Ethene), exchanges the coordinated ethene with ethene in solution. This exchange does not only occur during the course of the thermal decomposition. If [**1**]Pt(Ethene-d^4) dissolved in toluene is left under an atmosphere of unlabeled ethene, exchange of the coordinated ethene-d^4 by unlabeled ethene is observed at room temperature after 30 min. We were interested whether this exchange is a dissociative or an associative process since this is essential for our basic strategy outlined in Scheme 2. If the process is dissociative, compound **3** in Scheme 2 must at least be temporarily available and, thus the entrance to sub-equilibrium (**D**) in Scheme 2 is open. As can be seen from Fig. 6 which shows an excerpt of the ^{1}H NMR spectrum of [**1**]Pt(Ethene) in the range of 1.5–5.5 ppm at different temperatures, this investigation could be done by ^{1}H-VT NMR measurement through line shape analysis.

Fig. 6 shows that with increasing temperature both the peak for free ethene at 5.25 ppm and that for coordinated ethene at 1.8 ppm begin to broaden more and more. Free ethene alone, dissolved in toluene-d^8, did not show any broadening when performing the same measurement. This control experiment also served to receive the natural line width at half height of the peak of free ethene which was found to be 2.75 Hz. The measurement was done at different concentrations of ethene. The concentration of it was received via integration of the peak for free ethene and that of coordinated ethene (Fig. 6). The latter concentration was known through the experimental settings. The evaluation was performed analogously to a similar exchange problem (exchange of the center metal in crown ethers) which is published [13]. The line shape of the peak of free ethene was fitted using the equations in [13b,c]. The parameters to be fitted were the intensity of the peak and the averaged life time τ over both positions (free and coordinated ethene) as described in [13b,c]. Table 5 shows the τ values received from the curve fit at different concentrations of ethene and different temperatures. Fig. 7 shows an example of the curve fit.

Using Eq. (1) [13a], both the associative and the dissociative kinetic parameters for the exchange of ethene in [**1**]Pt(Ethene) could be extracted (Table 5)

$$1/(\tau[\text{ethene}]_{\text{total}}) = k_{\text{diss}}/[\text{ethene}]_{\text{free}} + k_{\text{ass}}. \quad (1)$$

Fig. 8 shows the plots according to Eq. (1) and Fig. 9 shows the Eyring plot using the data of Table 5. It should be pointed out that the large uncertainty for the k_{ass} values is an intrinsic problem of a curve fit in which the experimental data show up as inverse parameters ($1/(\tau\ [\text{ethene}]_{\text{total}})$, $1/[\text{ethene}]_{\text{free}}$).

From Fig. 9 the activation parameters $\Delta_{\text{diss}}H^{\ddagger} = 86.0 \pm 6.5$ kJ/mol and $\Delta_{\text{diss}}S^{\ddagger} = 5.4 \pm 17.8$ J/(mol K) as well as $\Delta_{\text{ass}}H^{\ddagger} = 26.9 \pm 29.6$ kJ/mol and $\Delta_{\text{ass}}S^{\ddagger} = -148.0 \pm 87.5$ J/(mol K) are received. These values are

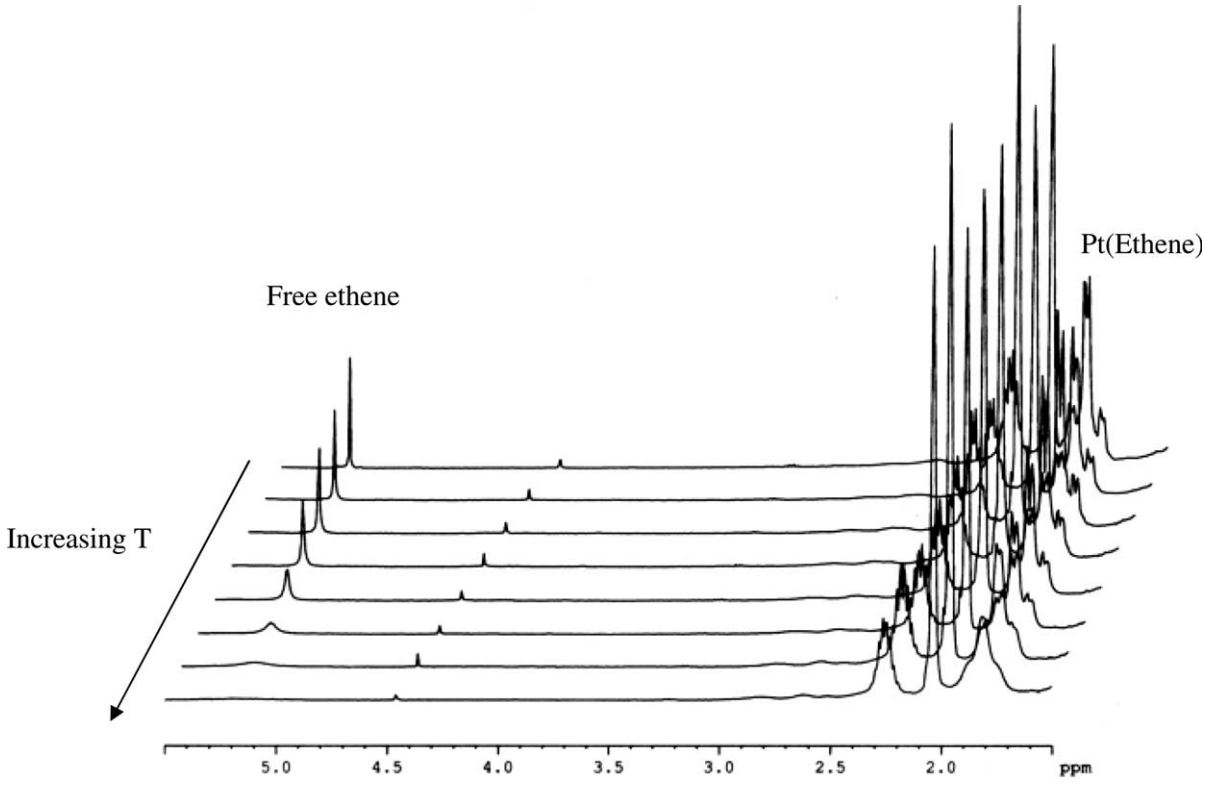

Fig. 6. ^{1}H NMR spectrum of [**1**]Pt(Ethene) with added free ethene at different temperatures.

in accordance with the expectation that the dissociative barrier should be enthalpically dominated with a positive activation entropy while in the associative pathway the barrier is entropically dominated with a low activation enthalpy. It is to be mentioned that $\Delta_{scram}H^{\ddagger}$ in [**1**]PtEt$_2$ is lower than $\Delta_{diss}H^{\ddagger}$ is in [**1**]Pt(Ethene). This can be taken as an additional explanation why the scrambling in [**1**]PtEt$_2$ occurs strictly intramolecularely, though the electronic situation in both cases is, of course, not completely comparable. We had expected $\Delta_{diss}S^{\ddagger}$ to be somewhat larger. The value determined speaks in favor of an early transition state. The data found are an indirect evidence that compound **3** in Scheme 2 exists temporarily. The data are unequivocally good enough to state that both pathways (associative and dissociative) take place; the dissociation of ethene from (PPh$_3$)$_2$Pt(Ethene) and (PCy$_3$)$_2$Pt(Ethene) in solution has been reported [14].

To further support the existence of **3** in Scheme 2, we tried [**1**]Pt(Ethene) in several test reactions with substrates that usually react with L$_2$Pt(0) compounds (Scheme 11).

[**1**]Pt(Ethene), when heated on air at 353 K for 4 h yields quantitatively into [**1**]PtO$_2$ complex (δ_P = 124.1 ppm, $^{1}J_{PPt}$ = 4145.6 Hz, δ_{Pt} = −4219.2 ppm, IR: 1634.4 cm^{-1} (s)). If [**1**]Pt(Ethene) is stirred at room temperature under an atmosphere of H$_2$, [**1**]PtH$_2$ can be detected (δ_P = 183.8 ppm (br), $^{1}J_{PPt}$ = 1091.7 Hz, δ_H = −3.43 ppm (br), $^{1}J_{PtH}$ = 1029.5 Hz, $^{2}J_{PH\,cis}$ = 121.3 Hz, $^{2}J_{PH\,trans}$ = 31.8 Hz), but it is not stable enough to be isolated. If [**1**]Pt(Ethene) is stirred at room temperature with excess of H$_2$SiPh$_2$, [**1**]Pt(H)(SiHPh$_2$) is formed quantitatively (δ_{Pa} = 181.5 ppm, δ_{Pb} = 190.9 ppm $^{1}J_{PaPt}$ = 1961.6 Hz, $^{1}J_{PbPt}$ = 2867.0 Hz, $^{2}J_{PaPb}$ = 22.7 Hz (P$_a$ *trans* to H, P$_b$ *trans* to SiHPh$_2$), δ_H = −2.78 ppm, $^{1}J_{PtH}$ = 844.3 Hz, $^{2}J_{PH\,cis}$ = 161.8 Hz, $^{2}J_{PH\,trans}$ = 31.9 Hz). If [**1**]Pt(Ethene) is treated with 1 eq of MeI the slow appearance of a new broad pseudo-triplet in ^{31}P NMR spectroscopy is observed at 153.5 ppm ($^{1}J_{PPt}$ = 3101.7 Hz) in the range of minutes, which is accompanied with a broad pseudo-triplet in the ^{1}H NMR spectrum at −12.5 ppm ($^{n}J_{PtH}$ = 1308.9 Hz) and a peak at 5.25 ppm for free ethene. This reaction does not go to completion. We ascribe these peaks to the structure shown in Scheme 11 resulting from a methyl transfer onto the Pt forming a {[**1**]PtMe^{+}I^{-}} ion pair. This would be in accordance with the assumption that the oxidative addition of MeI should be a non-concerted two-step process. Since the back-side attack of the I^{-} anion in the second step is blocked through the biphenyl backbone of [**1**], the oxidative addition is trapped after the first step (methyl transfer). A similar structure has been proposed by Stille for a Pd(II) complex [16]. Since the J_{PtH} coupling constant of 1309.8 Hz is too large for a ^{2}J coupling, we propose that an interaction of the methyl's H atoms with the Pt center must be present ($^{1}J_{PtH}$ coupling constants of the magnitude found are not uncommon) with a free rotation axis along the Pt–C connection which leads to no visible J_{PH} coupling.

Table 5
Quantitative data for the evaluation of the ethene exchange behavior of [**1**]Pt(Ethene)

T (K)	Total ethene (mol/L)	Free ethene (mol/L)	Exchange time τ (s)	k_{diss} (1/s)	k_{ass} (L/(mol s))
333	0.0488	0.00279	0.12 ± 0.02	0.448 ± 0.019	8.3 ± 5.9
	0.064	0.0038	0.07 ± 0.02		
	0.07	0.011	0.3 ± 0.2		
	0.0732	0.0122	0.3 ± 0.2		
	0.093	0.032	0.3 ± 0.2		
	0.105	0.044	0.3 ± 0.2		
343	0.0488	0.00279	0.045 ± 0.01	1.221 ± 0.061	10.0 ± 19.1
	0.064	0.0038	0.05 ± 0.01		
	0.07	0.011	0.10 ± 0.05		
	0.0732	0.0122	0.11 ± 0.07		
	0.093	0.032	0.12 ± 0.02		
	0.105	0.044	0.5 ± 0.15		
	0.178	0.117	0.40 ± 0.15		
353	0.0488	0.00279	0.025 ± 0.015	2.180 ± 0.111	11.7 ± 45.4
	0.064	0.0038	0.03 ± 0.015		
	0.07	0.011	0.065 ± 0.02		
	0.0732	0.0122	0.08 ± 0.01		
	0.093	0.032	0.07 ± 0.02		
	0.105	0.044	0.25 ± 0.02		
	0.178	0.117	0.15 ± 0.07		
363	0.0488	0.00279	0.0085 ± 0.002	6.637 ± 0.084	20.3 ± 25.2
	0.064	0.0038	0.009 ± 0.002		
	0.07	0.011	0.025 ± 0.005		
	0.0732	0.0122	0.025 ± 0.005		
	0.093	0.032	0.034 ± 0.008		
	0.105	0.044	0.072 ± 0.02		
	0.178	0.117	0.080 ± 0.009		
373	0.0488	0.00279	0.0045 ± 0.002	12.433 ± 0.490	30.8 ± 147.0
	0.064	0.0038	0.005 ± 0.002		
	0.07	0.011	0.012 ± 0.003		
	0.0732	0.0122	0.015 ± 0.005		
	0.093	0.032	0.017 ± 0.003		
	0.105	0.044	0.024 ± 0.002		
	0.178	0.117	0.045 ± 0.009		

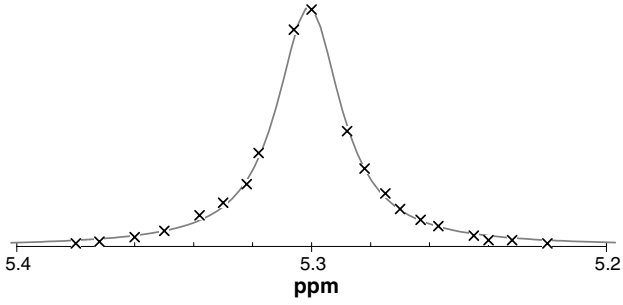

Fig. 7. Curve fit of the ^{1}H NMR spectrum with $[ethene]_{total}$ = 0.105 mol/L, $[ethene]_{free}$ = 0.044 mol/L and T = 373 K. τ was received to be 0.024 s.

Concerning sub-equilibrium (**C**) in Scheme 2 it can, thus, be stated that the equilibrium is far on the left but partially and temporarily (**3**) is formed via dissociation of ethene, thus, opening up the pathway to sub-equilibrium (**D**) in Scheme 2.

Performing the thermolysis of [**1**]Pt(Ethene) the C–C activated compound **5** in Scheme 2 could never be isolated or detected. Unfortunately, we did not succeed in synthesizing compound **5** of Scheme 2 by treating (COD)$PtCl_2$ with two equivalents of the *ortho*-metallated phosphinite 2-M–Ph(OP(*i*-Pr)$_2$), M = Li, MgI (Scheme 12) to prove that this compound is thermodynamically stable in the temperature range employed and to examine the back-reaction (reductive elimination) of sub-equilibrium (**D**) of Scheme 2.

The *ortho*-metallated phosphinite seems to rearrange to the phenolate shifting the phosphine into the *ortho*-position both for the Grignard and the lithium compound according to the ^{31}P NMR signal for the hydrolyzed product received when quenching the *ortho*-metallation attempt (starting material (*o*-I-phenyl)–O–PR_2) with water at low temperatures (singulet in the negative δ-area).

Since we were not able to detect **3** or **5** of Scheme 2 we calculated the molecules and their thermodynamic

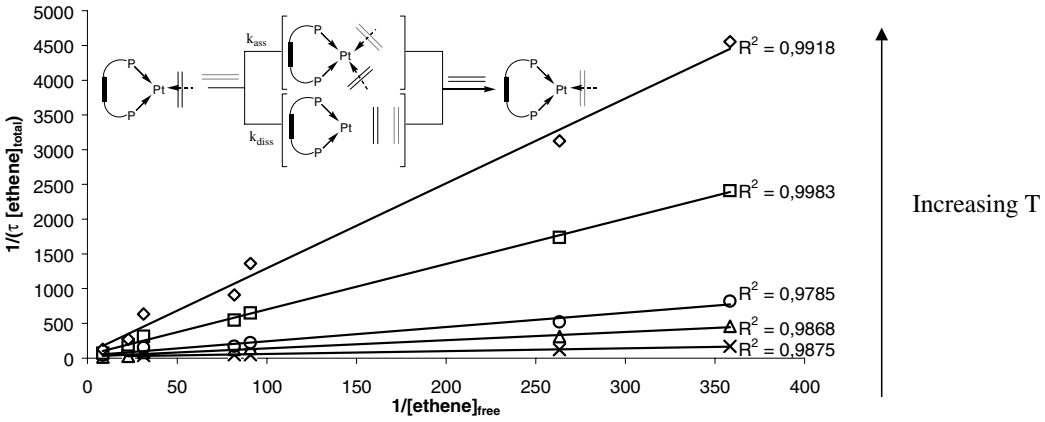

Fig. 8. Plots according to Eq. (1) with the data of Table 5.

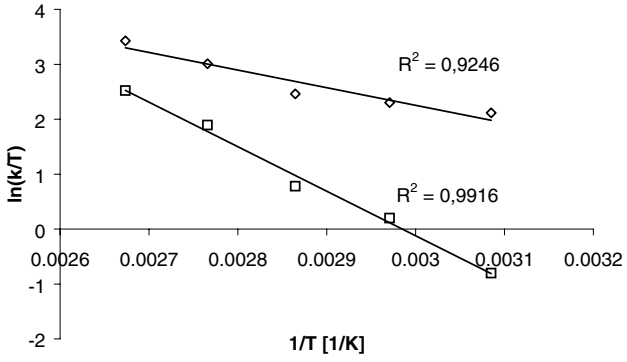

Fig. 9. Eyring plot for the dissociative (□) and the associative (◇) pathway in the ethene exchange of [**1**]Pt(Ethene).

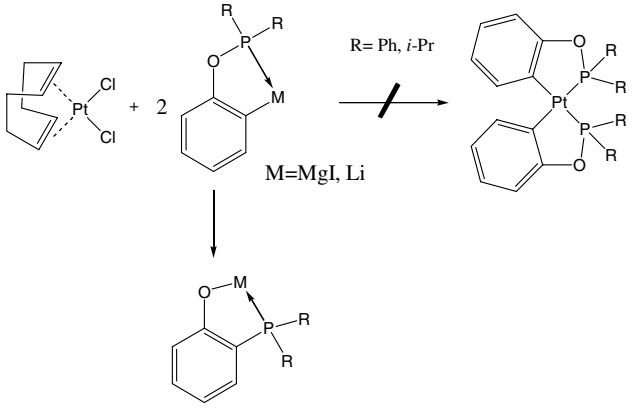

Scheme 12.

stability on the B3LYP/LANL2DZ level. Compound **3** was found as local minimum with a P–Pt–P of 150.8° and a distance of the Pt center to the bridging C atoms in the biphenyl fragment of 3.48 Å. According to these calculations the C–C activated product should be thermodynamically favored (both the *cis* and the *trans* product) in comparison to **3**. However, the calculations on the B3LYP/LANL2DZ level also predict **3** in Scheme 2 and free ethene to be more stable than **4** in Scheme 2 which is unequivocally wrong. This confirms our experience (not only remembering the low predictive power of the structure of [**1**]Pt(Ethene), demonstrated above)

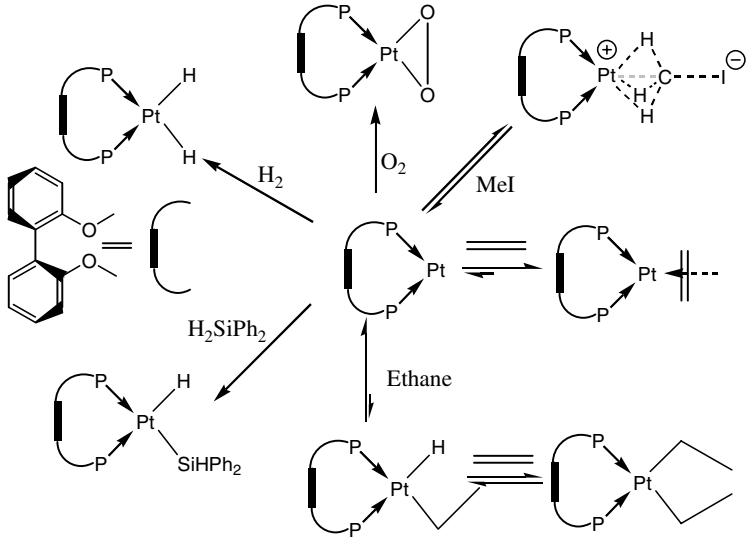

Scheme 11.

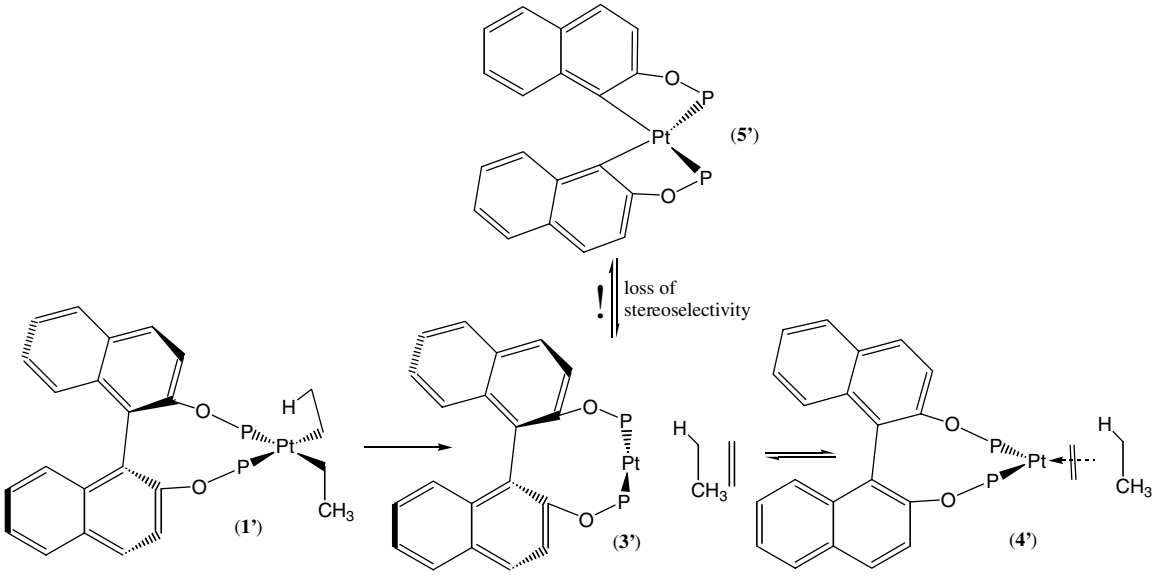

Scheme 13.

that the LANL2DZ basis set is critical to describe transition metals of the third row satisfactory both concerning the structure and the thermochemistry [15].

To still check whether the sub-equilibrium (**D**) in Scheme 2 exists but is invisible because compound **5** is too unstable to be observed, an indirect way for the detection was tried based on the potential loss of chirality of the axially chiral ligand backbone, if **5** is formed as intermediate (Scheme 13).

We did not try to synthesize ligand [**1**] enantioselectively but used ligand [**4**] instead for which the biphenol is available enantiomerically pure. [**4**]$PtCl_2$ and [**4**]$PtEt_2$ could both be synthesized and show large $[\alpha]^{Na}$ values of $-211.9°$ and $-230.3°$, respectively. The thermolysis of [**4**]$PtEt_2$ yielded cleanly into [**4**]Pt(Ethene). The kinetic is similar to that of [**1**]$PtEt_2$ but was not examined in detail. If the reaction is carried out at 363 K under an atmosphere of ethene to prevent a possible loss of stereoselectivity the product [**4**]Pt(Ethene) shows an $[\alpha]^{Na}$ of $-248.9°$ (the measurement was done in toluene saturated with ethene). If [**4**]Pt(Ethene) is heated in toluene-d^8 for 72 h (this was the longest time period we could heat a sample without significant amount of oxidation product, detected as a peak at 60 ppm in ^{31}P NMR spectroscopy, appeared) at 378 K, no significant decrease in $[\alpha]^{Na}$ was observed. Unfortunately, we must, thus, conclude that under the conditions employed not even temporarily the bridging C–C single bond is activated.

3. Conclusion

We must state that our initial target to activate the non-strained C–C bridge of the biphenyl fragment was not reached or at least that this reaction is decisively slower than 12 s^{-1} at 378 K (this is the dissociative exchange rate of the coordinated ethene). From this we conclude that the approach of the bridging C–C single bond to the metal center is not the most important part of the activation energy for the cleavage of that bond. A future strategy is to employ coordinated olefins which are more weakly bound (propene, *i*-butene) to offer the bridging C–C single bond more time to be activated. Electron-withdrawing groups on the biphenyl fragment should also increase the chance for an activation [3e]. By switching from Pt(0) to Pt(II) using [**1**]$PtMe^+$ as starting material the influence of the center metal's oxidation state is to be examined. As long as we are able to organize money for it, we will not stop trying to contribute our part to solve the problem of cleaving non-strained and non-activated C–C single bonds. Taking the positive side of our results we have proven that (**4′**) retains its stereochemical information even at elevated temperature. According to the high $[\alpha]^{Na}$ values the stereochemical information is distinctive. Remembering the activation reactions summarized in Scheme 11, we see a high potential in using the easily available and fairly stable (**4′**) in catalytic stereoselective reactions such as hydrogenation or hydrosilylation, which we are planning to examine in the nearest future.

4. Experimental

Manipulations and experiments were performed under an argon atmosphere using standard Schlenk techniques and/or in an argon-filled glove-box if not mentioned otherwise. Diethylether was distilled from benzophenone/sodium and stored under an argon atmosphere over molecular sieves. Dichloromethane, $CDCl_3$, pentane and

acetonitrile were degased with dinitrogen for 30 min, distilled and stored under argon over molecular sieves. K_2PtCl_4 and *S*-(−)-1,1′-Bi-2-naphthol were purchased from Strem Chemicals and used without further manipulation. Ethene 2.7 and dihydrogen 5.0 were received from Messer Grießheim and used as delivered. Ethane was generated by ethanolysis of ethyl Grignard. 1*Z*,5*Z*-cyclooctadiene (COD), chlorodiphenylphosphane, chlorodiisopropylphosphane, chlorodicyclohexylphosphane, 2,2′-dihydroxbiphenyl, ethyl-Grignard (2 M in diethelether), H_2SiPh_2, CD_3CD_2Br, CD_3COCl, $LiAlD_4$ and CH_3COBr were purchased from Aldrich and used without further purification. (COD)$PtCl_2$ was synthesized according to the literature [17].

The NMR measurement was performed on a Bruker AMX400. ^1H NMR (7.24 ppm, 400 MHz) and ^{13}C NMR (77.0 ppm, 100 MHz) spectra were referred to the $CDCl_3/CHCl_3$ resonances, ^{31}P NMR (161 MHz) to 85% H_3PO_4 as external standard, ^{195}Pt NMR (−3329 ppm, 85.6 MHz) to (COD)$PtCl_2$ as external standard. FTIR measurement was done on a JASCO FI7IR-460plus machine using KBr pellets. $[\alpha]^D$ data were determined on a Perkin–Elmer 241MC polarimeter.

4.1. General synthesis of the ligands

Route 1. 6 mmol of 2,2′-dihydroxybiphenyl were dissolved in 50 mL of diethylether. 23 mmol of triethylamine were added. Then 12.5 mmol of chlorodiphenylphosphine were added dropwise. Immediately, a white precipitation formed. It was stirred over night. The next day the white solid was removed by filtration and washed with 50 mL of diethylether. From the combined ether extracts the solvent was removed. A white solid resulted.

Route 2. 6 mmol of 2,2′-dihydroxybiphenyl were dissolved in 40 mL of acetonitrile. 23 mmol of triethylamine were added. Then 12.5 mmol of chlorodialkylphosphine were added dropwise. It was then heated to 60 °C over night. During that time a white precipitate formed. The next day 40 mL of pentan were added and it was stirred for 1 h. Then the pentane phase was separated via cannula into a new flask from which the pentane was removed in vacuo to yield the ligand.

4.1.1. Biphen(OPi-Pr) [1]

Colorless oil (yield 85%). ^1H NMR ($CDCl_3$, ppm): 0.79–0.85 (24H, m, CH–CH_3), 1.61 (m, 4H, C*H*–CH_3), 6.87 (t, 2H, CH–arom.). $^{13}C\{^1H\}$ NMR ($CDCl_3$, ppm): 16.81 (d, $^2J_{CP}$ = 8.75 Hz, CH*C*H_3), 17.51 (d, $^2J_{CP}$ = 19.52 Hz, CH*C*H_3), 27.99 (d, $^1J_{CP}$ = 17.31 Hz, *C*HCH_3), 117.27 (d, $^3J_{CP}$ = 19.5 Hz) 120.58 (s), 128.17 (s), 129.51 (d, $^4J_{CP}$ = 1.2 Hz), 131.55 (s), 156.75 (d, $^2J_{CP}$ = 8.0 Hz, P–O–C). $^{31}P\{^1H\}$ NMR ($CDCl_3$, ppm): 147.67. EA Calc. for $C_{18}H_{36}O_2P_2$: C, 68.9; H, 8.7; P, 14.8. Found: C, 68.08; H, 8.62; P, 14.11%.

4.1.2. Ph(OPCy) [2]

White solid (yield 97%). ^1H NMR ($CDCl_3$, ppm): 1.05–1.95 (44H, m, Cy), 6.92 (2H, t, CH-arom.), 7.25 (2H, t, CH-arom.), 7.37 (2H, d, CH-arom.), 7.55 (2H, d, CH-arom.). $^{13}C\{^1H\}$ NMR ($CDCl_3$, ppm): 26.08 (d, J_{CP} = 12.4 Hz), 26.89 (s), 27.21 (s), 37.76 (d, $^1J_{CP}$ = 16.8 Hz), 117.52 (d, $^3J_{CP}$ = 19.0 Hz), 120.66 (s), 128.16 (s), 129.75 (s), 131.39 (s), 156.99 (d, $^2J_{CP}$ = 8.77 Hz, P–O–C). $^{31}P\{^1H\}$ NMR ($CDCl_3$, ppm):147.0 (s). EA Calc. for $C_{36}H_{52}O_2P_2$: C, 74.7; H, 9.1; P, 10.7. Found: C, 73.82; H, 9.19; P, 10.10%.

4.1.3. Biphen(OPPh) [3]

White solid (yield 95%). ^1H NMR ($CDCl_3$, ppm): 7.02–7.26 (m). $^{13}C\{^1H\}$ NMR ($CDCl_3$, ppm): 118.2 (d, $^3J_{CP}$ = 16.5 Hz), 122.31 (s), 128.15 (d, $^3J_{CP}$ = 17.9 Hz), 128.70 (s), 129.15 (s). 130.08 (d, $^3J_{CP}$ = 22.6 Hz), 131.44 (s), 141.37 (d, $^1J_{CP}$ = 17.9 Hz), 155.12 (d, $^2J_{CP}$ = 9.9 Hz, P–O–C). $^{31}P\{^1H\}$ NMR ($CDCl_3$, ppm): 112.8 (s). EA Calc. for $C_{36}H_{28}O_2P_2$: C, 78.0; H, 5.1; P, 11.2. Found: C, 78.8; H, 5.14; P, 10.64%.

4.1.4. S-Naph(OPi-Pr) [4]

Viscose white oil (yield 92%). ^1H NMR ($CDCl_3$, ppm): 0.44 (3H, d $^3J_{HH}$ = 9.5 Hz, CHCH_3), 0.46 (3H, d $^3J_{HH}$ = 9.5 Hz, CHCH_3), 0.54 (3H, d $^3J_{HH}$ = 7.25 Hz, CHCH_3), 0.58 (3H, d $^3J_{HH}$ = 7.28 Hz, CHCH_3), 0.86 (12H, m, CHCH_3), 1.30 (2H, br hept, C*H*CH_3), 1.64 (2H, hept $^3J_{HH}$ = 7.21 Hz, C*H*CH_3), 7.16 (4H, m, Ar-H), 7.33 (2H, mm Ar-H), 7.72 (2H, br d $^3J_{HH}$ = 10.6 Hz, Ar-H), 7.95 (2H, d $^3J_{HH}$ = 9.3 Hz, Ar-H), 8.01 (2H, d $^3J_{HH}$ = 9.6 Hz, Ar-H). $^{13}C\{^1H\}$ NMR ($CDCl_3$, ppm): 15.72 (d, $^2J_{CP}$ = 7.4 Hz), 17.10 (d, $^2J_{CP}$ = 6.2 Hz), 17.33 (d, $^1J_{CP}$ = 14.8 Hz), 17.40 (d, $^1J_{CP}$ = 21.0 Hz), 27.86 (d, $^1J_{CP}$ = 18.5 Hz), 27.69 (d, $^1J_{CP}$ = 16.0 Hz), 118.19 (d, $^3J_{CP}$ = 20.9 Hz), 120.84 (s), 123.50 (s), 125.94 (s), 126.01 (s), 127.79 (s), 128.77 (s), 129.32 (s), 134.21 (s), 153.97 (d, $^2J_{CP}$ = 8.6 Hz, P–O–C). $^{31}P\{^1H\}$ NMR ($CDCl_3$, ppm): 145.6 (s). EA Calc. for $C_{32}H_{40}O_2P_2$: C, 74.11; H, 7.77; P, 11.94. Found: C, 74.30; H, 7.99; P, 11.94%. $[\alpha]^{Na}_{25\,°C,toluene} = -64.7°$.

4.2. General synthesis of the $PtCl_2$ complexes

To a suspension of 0.3 mmol of (COD)$PtCl_2$ in 10 mL of CH_2Cl_2 was added a solution of 0.3 mmol of the ligand in 10 mL of CH_2Cl_2. The mixture was allowed to stir overnight. A clear solution resulted. The next day the solvent was removed in vacuo. A white solid remained which was washed with 10 mL of pentane and dried in vacuo.

4.2.1. [1]$PtCl_2$

White solid (yield 89%). ^1H NMR ($CDCl_3$, ppm): 0.86 (3H, d, $^2J_{HH}$ = 7.1 Hz, CH–CH_3), 0.90 (3H, d, $^2J_{HH}$ = 7.1 Hz, CH–CH_3), 1.08 (3H, d, $^2J_{HH}$ = 7.2 Hz,

CH–CH_3), 1.12 (3H, d, $^2J_{HH}$ = 7.4 Hz, CH–CH_3), 1.45–1.54 (12H, m, CH–CH_3), 2.46 (2H, m, CH–CH_3), 3.34 (2H, m, CH–CH_3), 7.17 (2H, d, $^2J_{HH}$ = 8.0 Hz, CH-arom.), 7.29 (2H, t, $^2J_{HH}$ = 7.4 Hz, CH-arom.), 7.37–7.42 (4H, m, CH-arom.). $^{13}C\{^1H\}$ NMR ($CDCl_3$, ppm): 18.05 (s, CHCH$_3$), 18.15 (s, CHCH$_3$), 18.86 (s, CHCH$_3$), 19.94 (s, CHCH$_3$), 32,76 (d, $^1J_{CP}$ = 35.5 Hz, CHCH$_3$), 34.05 (d, $^1J_{CP}$ = 35.7 Hz, CHCH$_3$), 120.78 (s), 125.37 (s), 129.69 (s), 130.15 (s), 132.36 (s), 150.90 (d, $^2J_{CP}$ = 13.2 Hz, P–O–C). $^{195}Pt\{^1H\}$ NMR ($CDCl_3$, ppm): −4122.8 (t, $^1J_{PPt}$ = 4147.2 Hz). $^{31}P\{^1H\}$ NMR ($CDCl_3$, ppm): 123.4 (s), 123.4 (d, $^1J_{PPt}$ = 4147.2 Hz). FT-IR (cm^{-1}): 3064 (w), 2967 (s), 2930 (s), 2871 (s), 1596 (w), 1568 (w), 1498 (s), 1476 (s), 1431 (s), 1384 (w), 1365 (w), 1242 (s), 1208 (s), 1127 (w), 1101 (s), 1047 (m), 1031 (m), 932 (s), 899 (s), 769 (s), 756 (s), 725 (w), 664 (m), 638 (m), 620 (m), 599 (m), 535 (m), 519 (m). EA Calc. for $C_{24}H_{36}Cl_2O_2P_2Pt$: C, 42.1; H, 5.3; P, 9.1; Cl, 10.36. Found: C, 41.73; H, 5.44; P, 9.35; Cl, 10.02%. MS (FAB, *m/z*): 648.3 (M − Cl, correct isotope pattern).

4.2.2. [2]$PtCl_2$

White solid (yield 67%). ^1H NMR ($CDCl_3$, ppm): 0.64–3.06 (44H, m, Cy), 7.11 (2H, d, $^2J_{HH}$ = 8.0 Hz, CH-arom.), 7.28 (2H, t, $^2J_{HH}$ = 7.44 Hz, CH-arom.), 7.38–7.43 (4H, m CH-arom.). $^{13}C\{^1H\}$ NMR ($CDCl_3$, ppm): 25.82 (s), 26.18 (s), 26.68 (d, $^2J_{CP}$ = 13.2 Hz), 27.31 (s), 27.97 (s), 29.34 (d, $^2J_{CP}$ = 15.1 Hz), 43.38 (d, $^1J_{CP}$ = 34 Hz), 44.84 (d, $^1J_{CP}$ = 34.1 Hz), 120.54 (d, $^3J_{CP}$ = 2.8 Hz), 125.06 (s), 129.78 (d, $^3J_{CP}$ = 3.3 Hz), 130.10 (s), 131.23 (s), 151.26 (d, $^2J_{CP}$ = 14 Hz, P–O–C). $^{195}Pt\{^1H\}$($CDCl_3$, ppm): −4119.4 (t, $^1J_{PPt}$ = 4141.3 Hz). $^{31}P\{^1H\}$ NMR ($CDCl_3$, ppm): 118.7 (br s), 118.7 (br d, $^1J_{PPt}$ = 4141.3 Hz). FT-IR (cm^{-1}): 3064 (w), 2926 (s), 2851 (s), 1496 (m), 1476 (m), 1432 (m), 1249 (m), 1205 (m), 1101 (m), 1047 (w), 1004 (w), 942 (m), 894 (m), 851 (w), 768 (m), 731 (w), 589 (w). EA Calc. for $C_{18}H_{36}Cl_2O_2P_2Pt$: C, 51.2; H, 6.2; P, 7.3; Cl, 8.4. Found: C, 51.07; H, 6.10; P, 6.96; Cl, 8.40%.

4.2.3. [3]$PtCl_2$

White solid (yield 75%). ^1H NMR ($CDCl_3$, ppm): 6.78 (2H, d, $^2J_{HH}$ = 7.36 Hz, CH-arom.), 7.08–7.51 (28H, m CH-arom.). $^{13}C\{^1H\}$ NMR ($CDCl_3$, ppm): 122.24 (s), 125.80 (s), 127.88 (pseudo-t, J_{CPt} = 12.6 Hz), 127.92 (pseudo-t, J_{CPt} = 12.6 Hz), 129.71 (s), 130. 13 (s), 131. 42 (s), 131. 76 (s), 132.12 (s), 132.01 (m, overlapping with the peak at 132.12), 132.38 (d of pseudo-t, J_{CP} = 14.6 Hz, J_{CPt} = 14.4 Hz), 132.11 (s), 133.43 (s), 134.16 (s), 150. 73 (d, $^2J_{CP}$ = 8.85 Hz P–O–C). ^{195}Pt NMR ($CDCl_3$, ppm): −4150.7 (t, $^1J_{PPt}$ = 4230.4 Hz). $^{31}P\{^1H\}$ NMR ($CDCl_3$, ppm): 88.39 (s), 88.39 (d, $^1J_{PPt}$ = 4230.4 Hz). FT-IR (cm^{-1}): 3047.8 (w), 2955.2 (w), 2864.2 (w), 1645.9 (w), 1516.7 (m), 1463.7 (s), 1433.8 (m), 1269.9 (w), n1245.8 (w), 1206.3 (m), 1099.2 (s), 978.7 (s), 928.6 (m), 902.5 (m), 775.2 (m), 755.9 (w), 689.4 (s), 593.9 (w), 526.5 (s), 496.6 (m). EA Calc. for $C_{36}H_{28}Cl_2O_2P_2Pt$: C, 52.7; H, 3.4; P, 7.5; Cl, 8.6. Found: C, 52.29; H, 3.62; P, 7.11; Cl, 9.34%. MS (FAB, *m/z*): 748.3 (M − Cl, correct isotope pattern).

4.2.4. [4]$PtCl_2$

White solid (yield 76%). ^1H NMR ($CDCl_3$, ppm): 0.39 (3H, d $^3J_{HH}$ = 6.8 Hz, CHCH_3), 0.43 (3H, d $^3J_{HH}$ = 7.0 Hz, CHCH_3), 0.72 (3H, d $^3J_{HH}$ = 6.9 Hz, CHCH_3), 0.76 (3H, d $^3J_{HH}$ = 6.8 Hz, CHCH_3), 1.38 (3H, d $^3J_{HH}$ = 6.9 Hz, CHCH_3), 1.41 (3H, d $^3J_{HH}$ = 6.2 Hz, CHCH_3), 1.65 (3H, d $^3J_{HH}$ = 6.9 Hz, CHCH_3), 1.69 (3H, d $^3J_{HH}$ = 7.0 Hz, CHCH_3), 2.18 (2H, br hept, CHCH$_3$), 3.27 (2H, br hept, CHCH$_3$), 7.13 (2H, d $^3J_{HH}$ = 8.7 Hz, Ar-H), 7.29 (2H, t $^3J_{HH}$ = 8.2 Hz, Ar-H), 7.45 (2H, t $^3J_{HH}$ = 8.0 Hz, Ar-H), 7.50 (2H, d $^3J_{HH}$ = 8.5 Hz, Ar-H), 7.91 (2H, d $^3J_{HH}$ = 8.5 Hz, Ar-H), 7.99 (2H, d $^3J_{HH}$ = 8.7 Hz, Ar-H). $^{13}C\{^1H\}$ NMR ($CDCl_3$, ppm): 16.85 (s, CHCH$_3$), 18.30 (s, CHCH$_3$), 18.47 (s, CHCH$_3$), 20.85 (s, CHCH$_3$), 33.39 (d, $^1J_{CP}$ = 16.1 Hz, CHCH$_3$), 33.80 (d, $^1J_{CP}$ = 20.1 Hz, CHCH$_3$), 119.83 (s), 123.36 (s), 125.63 (s), 125.66 (s), 127.39 (s), 128.16 (s), 130.59 (s), 130.83 (s), 133.36 (s), 148.92 (d, $^2J_{CP}$ = 12.1 Hz, C–O–P). $^{195}Pt\{^1H\}$ NMR ($CDCl_3$, ppm): −4228.8 (t, $^1J_{PPt}$ = 4022.9 Hz). $^{31}P\{^1H\}$ NMR ($CDCl_3$, ppm): 127.5 (s), 127.5 (d, $^1J_{PPt}$ = 4022.9 Hz). FT-IR (cm^{-1}): 3053.0 (w), 2963 (w), 2926 (w), 2870 (w), 1587 (w), 1504 (w), 1567 (s), 1360 (w), 1228 (s), 1077 (m), 1028 (m), 991 (s), 880 (w), 826 (s), 748 (m), 693 (m). EA Calc. for $C_{32}H_{40}Cl_2O_2P_2Pt$: C, 48.99; H, 5.14; P, 7.89; Cl, 9.04. Found: C, 48.27; H, 5.07; P, 7.44; Cl, 9.90%. $[\alpha]^{Na}_{25\,^\circ C,toluene} = -211.9^\circ$. MS (FAB, *m/z*): 784.1 (M − Cl, correct isotope pattern).

4.3. General synthesis of the $PtEt_2$ complexes

0.15 mmol of [ligand]$PtCl_2$ were suspended in 5 mL of diethylether. The suspension was cooled to −30 °C. Then 0.45 mmol of ethylmagnesiumbromide in diethylether were added dropwise via syringe. The reaction mixture was stirred for 1 h. Then 0.5 mL of 1,4-dioxane were added and the white precipitate was removed by filtration through aluminium oxide and washed with 10 mL of diethylether. From the combined ether extracts the solvent was removed in vacuo. An off-white solid resulted.

4.3.1. [1]$PtEt_2$

White solid (yield 62%). ^1H NMR (toluene-d^8, ppm): 0.61 (3H, d, $^2J_{HH}$ = 7.3 Hz, CH–CH_3), 0.65 (3H, d, $^2J_{HH}$ = 7.2 Hz, CH–CH_3), 0.88 (3H, d, $^2J_{HH}$ = 7.2 Hz, CH–CH_3), 0.91 (3H, d, $^2J_{HH}$ = 7.3 Hz, CH–CH_3), 0.86–1.34 (10H, m, Ethyl), 1.34–1.39 (12H, m, CH–CH_3), 2.06 (2H, m, CH–CH_3), 2.66 (2H, m, CH–CH_3),

7.03 (2H, d, $^{2}J_{HH}$ = 8.1 Hz, CH-arom.), 9.1 (2H, t, $^{2}J_{HH}$ = 7.5 Hz, CH-arom.), 7.23–7.26 (4H, m, CH-arom.). $^{13}C\{^{1}H\}$ NMR (toluene-d^8, ppm): 13.50 (dd, $^{2}J_{CPcis}$ = 10.1 Hz, $^{2}J_{CPtrans}$ = 106.6 Hz, $^{1}J_{CPt}$ = 418.3 Hz, Pt–CH_2), 16.93 (t, $^{3}J_{CP}$ = 3.0 Hz, $^{2}J_{CPt}$ = 22.0 Hz, $PtCH_2$–CH_3), 17.60 (pseudo–t, J_{CPt} = 65.4 Hz, $PCHCH_3$), 18.41 (pseudo–t, J_{CPt} = 99.6 Hz, $PCHCH_3$), 18.48 (pseudo–t, J_{CPt} = 50.3 Hz, $PCHCH_3$), 19.84 (pseudo –t, J_{CPt} = 80.5 Hz, J_{CPt} = 17.3 Hz, $PCHCH_3$), 31.29 (d with pseudo-t, $^{1}J_{CP}$ = 18.49 Hz, J_{CPt} = 17.3 Hz, $PCHCH_3$), 31.88 (d with pseudo-t, $^{1}J_{CP}$ = 24.66 Hz, J_{CPt} = 17.2 Hz, $PCHCH_3$), 121.38 (s), 124.59 (s), 131.47 (s), 132.52 (s), 153.80 (pseudo-t, J_{CPt} = 8.85 Hz). $^{195}Pt\{^{1}H\}$ NMR (toluene-d^8, ppm): −4494.2 (t, $^{1}J_{PPt}$ = 1971.4 Hz). $^{31}P\{^{1}H\}$ NMR (toluene-d^8, ppm): 159.40 (s), 159.40 (d, $^{1}J_{PPt}$ = 1971.4 Hz). FT-IR (cm^{-1}): 3066 (w), 2924 (s), 2853 (s), 1466 (m), 1378 (w), 1261 (m), 1207 (m), 1103 (m), 1019 (m), 903 (w), 802 (w), 759 (w), 677 (w), 464 (w). EA Calc. for $C_{28}H_{46}O_2P_2Pt$: C, 50.1; H, 6.9; P, 9.2. Found: C, 50.58; H, 6.98; P, 8.78%. MS (FAB, *m/z*): 614.3 (100%, M − ethane).

4.3.2. *[2]PtEt$_2$*

White solid (yield 49%). ^{1}H NMR ($CDCl_3$, ppm): 0.5–2.44 (54H, m, Cy and Ethyl), 6.97 (2H, d, $^{2}J_{HH}$ = 7.5 Hz, CH-arom.), 7.10 (2H, t, $^{2}J_{HH}$ = 7.3 Hz, CH-arom.), 7.24 (4H, m, CH-arom.). $^{13}C\{^{1}H\}$ NMR ($CDCl_3$, ppm): 12.53 (dd with pseudo-t, $^{2}J_{PCcis}$ = 107.6 Hz, $^{2}J_{PCtrans}$ = 10.2 Hz, $^{1}J_{CPt}$ = 635.0 Hz, Pt–CH_2), 16.04 (t with pseudo-t, $^{3}J_{CP}$ = 2.6 Hz, $^{2}J_{CPt}$ = 22.4 Hz, Pt–CH_2–CH_3), 17.61 (pseudo-t, J_{CPt} = 11.3 Hz, $PCHCH_3$), 18.40 (pseudo-t, J_{CPt} = 15.1 Hz, $PCHCH_3$), 18.48 (pseudo-t, J_{CPt} = 7.5 Hz, $PCHCH_3$), 19.82 (pseudo-t, J_{CPt} = 14.6 Hz, $PCHCH_3$), 31.28 (d with pseudo-t, $^{1}J_{CP}$ = 17.1 Hz, J_{CPt} = 17.0 Hz, P–CH–CH_3), 31.94 (d with pseudo-t, $^{1}J_{CP}$ = 24.1 Hz, J_{CPt} = 16.1 Hz, P–CH–CH_3), 120.93 (s), 123.14 (s), 128.77 (s), 131.08 (s), 131.85 (s), 153.22 (pseudo-t, 10.1 Hz, C–O–P). $^{195}Pt\{^{1}H\}$ NMR (toluene-d^8, ppm): −4464.7 (t, $^{1}J_{PPt}$ = 1945.7 Hz). $^{31}P\{^{1}H\}$ NMR ($CDCl_3$, ppm): 150.4 (s), 150.4 (d, $^{1}J_{PPt}$ = 1945.7 Hz). FT-IR (cm^{-1}): 3064 (w), 2927 (s), 2848 (s), 1497 (m), 1473 (m), 1444 (m), 1253 (m), 1216 (m), 1101 (m), 910 (m), 850 (w), 815 (w), 757 (m), 664 (w), 497 (w). EA Calc. for $C_{40}H_{62}O_2P_2Pt$: C, 57.75; H, 7.51; P, 7.45. Found: C, 57.79; H, 7.61; P, 7.87%.

4.3.3. *[3]PtEt$_2$*

White solid (yield 56%). ^{1}H NMR (toluene-d^8, ppm): 1.21 (6H, pseudo-t with d of t, $^{3}J_{HH}$ = 8.6 Hz, $^{3}J_{PtH}$ = 57.6 Hz, $^{4}J_{PH}$ = 8.6 Hz, CH_2–CH_3), 1.64 (4H, dd of q with pseudo-t, $^{3}J_{HH}$ = 8.6 Hz, $^{2}J_{PtH}$ = 105.4 Hz, $^{3}J_{PHcis}$ = 67.2 Hz, $^{3}J_{PHtrans}$ = 2.8 Hz, CH_2–CH_3), 6.54 (2H, dd, J_{HH} = 7.6 Hz, J_{HH} = 1.8 Hz, backbone phenyl-H), 6.62 (2H, t, J_{HH} = 7.6 Hz backbone phenyl-H), 6.80 (2H, t, J_{HH} = 7.3 Hz, backbone phenyl-H), 6.84 (2H, dd, J_{HH} = 7.3, J_{HH} = 1.8 Hz, backbone phenyl-H), 7.02 (8H, pseudo-t, phenyl-H), 7.36 (6H, pseudo-t, phenyl-H), 7.46 (6H, pseudo-t, phenyl-H). $^{13}C\{^{1}H\}$ NMR ($CDCl_3$, ppm): 15.47 (pseudo-t with t, $^{3}J_{CP}$ = 1.7 Hz, $^{2}J_{CPt}$ = 14.4 Hz, $PtCH_2$–CH_3), 16.47 (dd, $^{2}J_{CPcis}$ = 10.9 Hz, $^{2}J_{CPtrans}$ = 120.7 Hz, $^{1}J_{CPt}$ = 643.9 Hz, Pt–CH_2), 122.2 (s), 124.2 (s), 127.50 (pseudo-t, J_{CPt} = 10.3 Hz, *ortho*-C of PPh), 127.66 (pseudo-t, J_{CPt} = 8.7 Hz, *ortho*-C of PPh), 128.48 (s), 130.05 (s), 130.91 (pseudo-t, J_{CPt} = 11.2 Hz, *ortho*-C of PPh), 131.30 (s), 131.419 (s), 132.33 (pseudo-t, J_{CPt} = 15.6, *ortho*-C of PPh), 137.11 (d with pseudo-t, $^{1}J_{CP}$ = 45.3 Hz, J_{CPt} = 43.0 Hz, P-*C*), 138.21 (d with pseudo-t, $^{1}J_{CP}$ = 39.7 Hz, J_{CPt} = 44.1 Hz, P-*C*), 152.64 (pseudo-t, J_{CPt} = 8.6 Hz, P–O–C). $^{195}Pt\{^{1}H\}$ NMR (toluene-d^8, ppm): −4460.0 (t, $^{1}J_{PPt}$ = 1937.1 Hz). $^{31}P\{^{1}H\}$ NMR (toluene-d^8, ppm): 123.8 (s), 123.8 (d, $^{1}J_{PPt}$ = 1937.1 Hz). EA Calc. for $C_{40}H_{38}O_2P_2Pt$: C, 59.48; H, 4.74; P, 7.67. Found: C, 59.32; H, 4.65; P, 7.97%.

4.3.4. *[4]PtEt$_2$*

White solid (yield 64%). ^{1}H NMR (toluene-d^8, ppm): 0.17 (3H, d, $^{3}J_{HH}$ = 7.4 Hz, $CHCH_3$), 0.21 (3H, d, $^{3}J_{HH}$ = 7.4 Hz, $CHCH_3$), 0.56 (3H, d, $^{3}J_{HH}$ = 7.4 Hz, $CHCH_3$), 0.59 (3H, d, $^{3}J_{HH}$ = 7.2 Hz, $CHCH_3$), 1.04 (3H, d, $^{3}J_{HH}$ = 7.4 Hz, $CHCH_3$), 1.31 (3H, d, $^{3}J_{HH}$ = 7.4 Hz, $CHCH_3$), 1.37 (3H, d, $^{3}J_{HH}$ = 7.4 Hz, $CHCH_3$), 1.37 (3H, d, $^{3}J_{HH}$ = 7.4 Hz, $CHCH_3$), 1.41 (3H, d, $^{3}J_{HH}$ = 7.4 Hz, $CHCH_3$), 1.31–1.41 (10H, m, Pt-CH_2CH_3), 1.67 (2H, hept, $^{3}J_{HH}$ = 7.4 Hz, $CHCH_3$), 2.40 (2H, hept, $^{3}J_{HH}$ = 7.4 Hz, $CHCH_3$), 6.94 (2H, d $^{3}J_{HH}$ = 9.8 Hz, Ar-H), 7.13 (2H, t $^{3}J_{HH}$ = 7.4 Hz, Ar-H), 7.21 (2H, d $^{3}J_{HH}$ = 9.8 Hz, Ar-H), 7.36 (2H, d $^{3}J_{HH}$ = 7.3 Hz, Ar-H), 7.62 (4H, d $^{3}J_{HH}$ = 7.4 Hz, Ar-H). $^{13}C\{^{1}H\}$ NMR ($CDCl_3$, ppm): 13.76 (dd with pseudo-t, $^{1}J_{CPt}$ = 576.0 Hz, $^{2}J_{CPcis}$ = 103.6 Hz, $^{2}J_{CPtrans}$ = 10.1 Hz, Pt–CH_2), 16.08 (t with pseudo-t, $^{3}J_{CP}$ = 3.0 Hz, $^{2}J_{CPt}$ = 19.7 Hz, Pt–CH_2CH_3), 16.60 (pseudo-t, J_{CPt} = 15.8 Hz, PCH–CH_3), 16.60 (pseudo-t, J_{CPt} = 9.8 Hz, PCH–CH_3), 18.22 (pseudo-t, J_{CPt} = 15.8 Hz, PCH–CH_3), 18.70 (pseudo-t, J_{CPt} = 10.9 Hz PCH–CH_3), 20.52 (pseudo-t, JCPt=10.4 Hz PCH–CH_3), 31.38 (d with pseudo-t, $^{1}J_{CP}$ = 23.1 Hz, J_{CPt} = 46.3 Hz, $PCHCH_3$), 31.78 (d with pseudo-t, $^{1}J_{CP}$ = 28.2 Hz, J_{CPt} = 56.3 Hz, $PCHCH_3$), 122.00 (s), 122.93 (s), 124.70 (s), 125.52 (s), 126.45 (s), 127.67 (s), 129.20 (s), 130.65 (s), 133.92 (s), 151.45 (pseudo-t, J_{CPt} = 6.0 Hz, C–O–P). $^{195}Pt\{^{1}H\}$ NMR (toluene-d^8, ppm): −4636.1 (t, $^{1}J_{PPt}$ = 1968.8 Hz). $^{31}P\{^{1}H\}$ NMR (toluene-d^8, ppm): 162.1 (s), 162.1 (d, $^{1}J_{PPt}$ = 1968.8 Hz). $C_{36}H_{50}O_2P_2Pt$: C, 56.02; H, 6.53; P, 8.03. Found: C, 55.97; H, 6.60; P, 8.52%. $[\alpha]^{Na}_{25\,^{\circ}C,toluene} = -230.3^{\circ}$.

4.4. General procedure for the thermal decomposition

Between 15 and 80 mg of [ligand]$PtEt_2$ were dissolved in 0.5 mL of toluene-d^8 and put into a J. Young NMR

tube. The NMR tube was heated in an oil bath for defined time periods. The temperature was regulated by a contact thermometer and double-checked by a digital thermometer in the oil bath. The temperature was constant up to ±1 °C. After a defined time period the sample was taken out of the oil bath and cooled down in an ice bath. Then the sample was measured by means of ^{1}H and ^{31}P NMR spectroscopy and put back into the oil bath.

4.4.1. [1]Pt(Ethene)

Off-white solid (yield quantitative). ^{1}H NMR (toluene-d^8, ppm): 0.74 (12H, m, CH–CH_3), 1.055 (3H, d, $^{2}J_{HH}$ = 7.2 Hz, CH–CH_3), 1.09 (3H, d, $^{2}J_{HH}$ = 7.3 Hz, CH–CH_3), 1.20 (3H, d, $^{2}J_{HH}$ = 6.9 Hz, CH–CH_3), 1.29 (3H, d, $^{2}J_{HH}$ = 6.5 Hz, CH–CH_3), 1.34 (2H, hept, $^{2}J_{HH}$ = 7.1 Hz, CH–CH$_3$), 1.88 (4H, m, $^{2}J_{HPt}$ = 90 Hz, CH$_2$), 2.22 (, 2H, hept, $^{2}J_{HH}$ = 6.3 Hz, CH–CH_3), 6.82 (2H, t, $^{2}J_{HH}$ = 7.4 Hz, CH-arom.), 6.9–7.23 (6H, m, CH-arom.). $^{13}C\{^{1}H\}$ NMR (toluene-d^8, ppm): 16.75 (pseudo-t, $^{1}J_{CPt}$ = 17.6 Hz, ethene-C), 16.91 (pseudo-t, J_{CPt} = 7.3 Hz, CHCH$_3$), 17.41 (pseudo-t, J_{CPt} = 5.8 Hz, CHCH$_3$), 17.80 (pseudo-t, J_{CPt} = 20.5 Hz, CHCH$_3$), (one CH$_3$ group overlayed by solvent peak), 27.23 (d of pseudo-t, $^{1}J_{CP}$ = 25.6 Hz, J_{CPt} = 27.0 Hz, CHCH$_3$), 33.15 (d of pseudo-t, $^{1}J_{CP}$ = 52.7 Hz, J_{CPt} = 29.3 Hz, CHCH$_3$), 122.29 (s), 122.78 (s), 131.29 (pseudo-t, J_{CPt} = 22.4 Hz, *ortho-C*H), 132.95 (s, bridging C–C), 153.97 (br pseudo-t). $^{195}Pt\{^{1}H\}$ NMR (toluene-d^8, ppm): −5105.4 (t, $^{1}J_{PPt}$ = 4060.73 Hz). $^{31}P\{^{1}H\}$ NMR (toluene-d^8, ppm): 186.7 (s), 186.7 (d, $^{1}J_{PPt}$ = 4060.7 Hz). FT-IR (cm^{-1}): 3064 (w), 2959 (s), 2926(s), 2878 (s), 1575 (w), 1455 (m), 1384 (m), 1261 (s), 1209 (s), 1101 (s), 1022 (s), 881 (s), 802 (s), 765 (s), 664 (m), 505 (w). EA Calc. for $C_{26}H_{40}O_2P_2Pt$: C, 48.7; H, 6.28; P, 9.65. Found: C, 48.10; H, 6.31; P, 9.10%.

4.4.2. [4]Pt(Ethene)

^{1}H NMR (toluene-d^8, ppm): 0.24 (3H, d, $^{3}J_{HH}$ = 7.3 Hz, CHCH_3), 0.28 (3H, d, $^{3}J_{HH}$ = 7.3 Hz, CHCH_3), 0.47 (3H, d, $^{3}J_{HH}$ = 7.4 Hz, CHCH_3), 0.51 (3H, d, $^{3}J_{HH}$ = 7.3 Hz, CHCH_3), 0.92 (2H, hept, $^{3}J_{HH}$ = 7.3 Hz, CHCH$_3$), 1.04 (3H, d, $^{3}J_{HH}$ = 7.4 Hz, CHCH_3), 1.07 (3H, d, $^{3}J_{HH}$ = 7.3 Hz, CHCH_3), 1.27 (3H, d, $^{3}J_{HH}$ = 7.4 Hz, CHCH_3), 1.31 (3H, d, $^{3}J_{HH}$ = 7.4 Hz, CHCH_3), 1.92 (2H, br s with d, $^{2}J_{PtH}$ = 53.9 Hz, ethene-H), 1.97 (2H, br s with d, $^{2}J_{PtH}$ = 53.9 Hz, ethene-H), 2.29 (2H, hept, $^{3}J_{HH}$ = 7.4 Hz, CHCH$_3$), 6.98 (2H, d, $^{3}J_{HH}$ = 14.7 Hz, Naph-H), 7.02 (2H, d, $^{3}J_{HH}$ = 7.3 Hz, Naph-H), 7.15 (2H, t, $^{3}J_{HH}$ = 9.8 Hz, Naph-H), 7.33 (2H, d $^{3}J_{HH}$ = 9.8 Hz, Naph-H), 7.40 (2H, d $^{3}J_{HH}$ = 9.8 Hz, Naph-H), 7.61 (2H, d $^{3}J_{HH}$ = 9.8 Hz, Naph-H). $^{13}C\{^{1}H\}$ NMR (toluene-d^8, ppm): 14.96 (pseudo-t, $^{1}J_{CPt}$ = 19.0 Hz, ethene-C), 16.14 (pseudo-t, J_{CPt} = 7.3 Hz, CHCH$_3$), 16.71 (pseudo-t, J_{CPt} = 3.6 Hz, CHCH$_3$), 18.00 (br pseudo-t, CHCH$_3$), 26.41 (d of pseudo-t, $^{1}J_{CP}$ = 26.3 Hz, $^{2}J_{CPt}$ = 19.9 Hz, CHCH$_3$), 32.75 (d of pseudo-t, $^{1}J_{CP}$ = 55.6 Hz, $^{2}J_{CPt}$ = 12.4 Hz, CHCH$_3$), 121.52 (s), 121.97 (s), 124.98 (s), 125.20 (s), 125.36 (s), 129.99 (s), 133.06 (s), 152 (br s). $^{195}Pt\{^{1}H\}$ NMR (toluene-d^8, ppm): −5188.4 (t, $^{1}J_{PPt}$ = 3999.7 Hz). $^{31}P\{^{1}H\}$ NMR (toluene-d^8, ppm): 186.3 (s), 186.3 (d, $^{1}J_{PPt}$ = 4000.7 Hz). $[\alpha]^{Na}_{25\,^{\circ}C,toluene} = -248.9^{\circ}$.

4.5. VT measurement with [1]Pt(Ethene)

An NMR tube containing 0.5 mL of toluene-d^8 and 20 mg of [**1**]Pt(Ethene) was placed into a Schlenk tube under ethene atmosphere. Then the ethene atmosphere was replaced by argon. Different concentrations of ethene were achieved by carefully evacuating the Schlenk tube and refilling with argon until the desired concentration of ethene determined by ^{1}H NMR spectroscopy was reached. The temperature control unit of the NMR machine was calibrated with a sample of 1,2 ethanediol [18]. The measurement was done in 10 K steps. The temperature was allowed to reach a constant level for 15 min at each step. The measurement was done both increasing the temperature from 333 to 373 K and by decreasing the temperature from 373 K to room temperature. The average value received from the "up" and "down" measurement was taken for the kinetic evaluation.

4.6. Single-crystal X-ray structure determination of compounds [1]PtCl$_2$, [1]PtEt$_2$, [1]Pt(Ethene), [3]PtCl$_2$ · CH$_2$Cl$_2$ and [3]PtEt$_2$ · 0.5C$_4$H$_{10}$O

Crystal data and details of the structure determination are presented in Table 6. Suitable single crystals for the X-ray diffraction study were grown from diethyl ether (for [ligand]Pt(Alk)$_n$) or pentane/dichloromethane (for [ligand]PtCl$_2$). A clear colorless plate (yellow prism, pale yellow fragment, colorless fragment, pale yellow fragment) was stored under perfluorinated ether, transferred in a Lindemann capillary, fixed, and sealed. Preliminary examination and data collection were carried out on an area detecting system (NONIUS, MACH3, κ-CCD) at the window of a rotating anode (NONIUS, FR951) and graphite monochromated Mo Kα radiation (λ = 0.71073 Å). The unit cell parameters were obtained by full-matrix least-squares refinement of 4860 (5522, 2463, 6481, 7385) reflections. Data collection were performed at 123 (173, 173, 173, 173) K (OXFORD CRYOSYSTEMS) within a θ-range of $1.79^{\circ} < \theta < 25.34^{\circ}$ ($2.22^{\circ} < \theta < 25.35^{\circ}$, $2.15^{\circ} < \theta < 25.33^{\circ}$, $2.11^{\circ} < \theta < 25.35^{\circ}$, $1.92^{\circ} < \theta < 25.36^{\circ}$). Measured with 4 (10, 9, 9, 9) data sets in rotation scan modus with $\Delta\varphi/\Delta\omega = 1.0^{\circ}$ ($\Delta\varphi/\Delta\omega = 2.0^{\circ}$, $\Delta\varphi/\Delta\omega = 2.0^{\circ}$, $\Delta\omega = 1.0^{\circ}$, $\Delta\varphi/\Delta\omega = 1.0^{\circ}$). A total number of 18640 (68991, 30027, 63970, 122675) intensities were integrated. Raw data were corrected for Lorentz, polarization,

Table 6
Crystallographic data for [**1**]$PtCl_2$, [**1**]$PtEt_2$, [**1**]Pt(Ethene), [**3**]$PtCl_2 \cdot CH_2Cl_2$ and [**3**]$PtEt_2 \cdot 0.5C_4H_{10}O$

Complex	[**1**]$PtCl_2$	[**1**]$PtEt_2$	[**1**]Pt(Ethene)	[**3**]$PtCl_2 \cdot CH_2Cl_2$	[**3**]$PtEt_2 \cdot 0.5C_4H_{10}O$
Formula	$C_{24}H_{36}Cl_2O_2P_2Pt$	$C_{28}H_{46}O_2P_2Pt$	$C_{26}H_{40}O_2P_2Pt$	$C_{37}H_{30}Cl_4O_2P_2Pt$	$C_{84}H_{86}O_5P_4Pt_2$
Formula weight	684.45	671.67	641.60	905.43	1689.57
Color/habit	Colorless/plate	Yellow/prism	Pale yellow/fragment	Colorless/fragment	Pale yellow/fragment
Crystal dimensions (mm^3)	$0.05 \times 0.15 \times 0.15$	$0.08 \times 0.10 \times 0.23$	$0.23 \times 0.25 \times 0.43$	$0.13 \times 0.25 \times 0.56$	0.12×0.34 0.42
Crystal system	Monoclinic	Monoclinic	Monoclinic	Monoclinic	Orthorhombic
Space group	$P2_1/c$ (No. 14)	$C2/c$ (No. 15)	$C2/c$ (No. 15)	$P2_1/n$ (No. 14)	$Pbca$ (No. 61)
a (Å)	9.9986(2)	33.1954(3)	12.0343(1)	8.9801(1)	9.9727(1)
b (Å)	14.6637(3)	9.5783(1)	15.3551(2)	24.5095(1)	21.1883(1)
c (Å)	18.5545(4)	18.5887(2)	13.9530(1)	15.7767(1)	34.3638(2)
β (°)	101.9791(13)	106.4384(5)	91.8165(5)	96.3945(3)	90
V ($Å^3$)	2661.15(10)	5668.79(10)	2577.05(4)	3450.81(5)	7261.23(9)
Z	4	8	4	4	4
T (K)	123	173	173	173	173
D_{calc} (g cm^{-3})	1.708	1.574	1.654	1.743	1.546
μ (mm^{-1})	5.613	5.085	5.589	4.502	3.990
$F(000)$	1352	2704	1280	1776	3384
θ Range (°)	1.79–25.34	2.22–25.35	2.15–25.33	2.11–25.35	1.92–25.36
Index ranges (h,k,l)	±12, ±17, ±22	±39, ±11, ±22	±14, ±18, ±16	±10, ±29, ±19	±12, ±25, ±41
Number of reflections collected	18640	68991	30027	63970	122675
Number of independent reflections/R_{int}	4865/0.050	5189/0.057	2368/0.035	6298/0.050	6634/0.050
Number of observed reflections ($I > 2(I)$)	4393	4103	2351	5920	6121
Number of data/restraints/parameters	4865/0/288	5189/0/482	2368/0/222	6298/0/415	6634/0/455
$R1/wR2$ ($I > 2(I)$)[a]	0.0311/0.0717	0.0216/0.0354	0.0104/0.0264	0.0182/0.0432	0.0201/0.0504
$R1/wR2$ (all data)[a]	0.0364/0.0739	0.0346/0.0381	0.0105/0.0265	0.0206/0.0441	0.0233/0.0517
Goodness-of-fit on F^2[a]	1.106	1.038	1.143	1.082	1.052
Largest difference in peak and hole (e $Å^{-3}$)	+1.72 and −1.14	+0.84 and −0.62	+0.41 and −0.46	+0.68 and −0.51	+0.89 and −0.73

[a] $R_1 = \sum(\|F_o| - |F_c\|)/\sum|F_o|$; $wR_2 = \{\sum[w(F_o^2 - F_c^2)^2]/\sum[w(F_o^2)^2]\}^{1/2}$; GOF $= \{\sum[w(F_o^2 - F_c^2)^2]/(n-p)\}^{1/2}$.

and, arising from the scaling procedure, for latent decay and absorption effects. After merging [$R_{int} = 0.050$ (0.057, 0.035, 0.050, 0.050)] a sum of 4865 (5189, 2368, 6298, 6634) (all data) and 4393 (4103, 2351, 5920, 6121) [$I > \sigma(I)$], respectively, remained and all data were used. The structures were solved by a combination of direct methods and difference Fourier syntheses. All non-hydrogen atoms were refined with anisotropic displacement parameters. Full-matrix least-squares refinements with 288 (482, 222, 415, 455) parameters were carried out by minimizing $\sum w(F_o^2 - F_c^2)^2$ with the SHELXL-97 weighting scheme and stopped at shift/err <0.001 (0.002, 0.001, 0.002, 0.002). The final residual electron density maps showed no remarkable features. Neutral atom scattering factors for all atoms and anomalous dispersion corrections for the non-hydrogen atoms were taken from International Tables for Crystallography. All calculations were performed on an Intel Pentium II PC, with the STRUX-V system, including the programs PLATON, SIR-92, and SHELXL-97 [19].

4.6.1. [1]$PtEt_2$, [1]Pt(Ethene)

All hydrogen atoms were found and refined with individual isotropic displacement parameters.

4.6.2. [1]$PtCl_2$, [3]$PtCl_2 \cdot CH_2Cl_2$, [3]$PtEt_2 \cdot 0.5C_4H_{10}O$

All hydrogen atoms were placed in ideal positions (riding model).

4.6.3. [1]Pt(Ethene)

Small extinction effects were corrected with the SHELXL-97 procedure [$\varepsilon = 0.00028(4)$]. The molecule is located on a crystallographic twofold axis.

4.6.4. [3]$PtEt_2 \cdot 0.5C_4H_{10}O$

The solvent molecule diethyl ether is disordered over two positions.

5. Supplementary material

Crystallographic data (excluding structure factors) for the structures reported in this paper have been deposited with the Cambridge Crystallographic Data Centre as supplementary publication Nos. CCDC-273528 ([**1**]$PtCl_2$), CCDC-273531 ([**1**]$PtEt_2$), CCDC-273530 ([**1**]Pt(Ethene)), CCDC-273532 ([**3**]$PtCl_2 \cdot CH_2Cl_2$), and CCDC-273529 ([**3**]$PtEt_2 \cdot 0.5C_4H_{10}O$). Copies of the data can be obtained free of charge on application to CCDC, 12 Union Road, Cambridge CB2 1EZ, UK (fax: +44 1223 336 033; e-mail: deposit@ccdc.cam.ac.uk).

Acknowledgements

K.R. thanks the Fonds der chemischen Industrie for a Liebig grant. K.R. thanks Prof. Dr. mult.

W.A. Herrmann for financial support. E.H. thanks R. Jaeger, S. Beer and S. Randoll for there help during the course of the X-ray measurements.

References

[1] (a) A.E. Shilov, G.B. Shul'pin, Chem. Rev. 97 (1997) 2879–2932;
(b) R.H. Crabtree, Chem. Rev. 85 (1985) 245–269;
(c) J. Halpern, Inorg. Chim. Acta 100 (1985) 41–48;
(d) G.W. Parshall, Acc. Chem. Res. 8 (1975) 113–117;
(e) A.E. Shilov, G.B. Shul'pin (Eds.), Activation and Catalytic Reactions of Saturated Hydrogencarbons in the Presence of Metal Complexes, Kluwer Academic Publishers, Dortrecht, 2000;
(f) J.A. Davies, P.L. Watson, J.F. Liebman, A. Greenberg (Eds.), Selective hydrocarbon activation, VCH, New York/Weinheim, 1990;
(g) P.W.N.M. van Leeuwen, K. Morokuma, J.H. van Lenthe (Eds.), Theoretical aspects of homogeneous catalysis, Kluwer Academic Publishers, Dotrecht, 1995;
(h) A.D. Ryabov, Chem. Rev. 90 (1990) 403–424;
(i) W.D. Jones, F.J. Feher, Acc. Chem. Res. 22 (1989) 91–100;
(j) B.A. Arndtsen, R.G. Bergman, T.A. Mobley, T.H. Peterson, Acc. Chem. Res. 28 (1995) 154–162;
(k) B. Rybtchinski, D. Milstein, Angew. Chem. Int. Ed. 38 (1999) 870–883;
(l) Chul-Ho Jun, Chem. Soc. Rev. 33 (2004) 610–618.

[2] J.A. Martinho, J.L. Beauchamp, Chem. Rev. 90 (1990) 629–688.

[3] (a) B.L. Edelbach, R.J. Lachicotte, W.D. Jones, J. Am. Chem. Soc. 120 (1998) 2843–2853;
(b) G. Ujaque, F. Maseras, O. Eisenstein, L. Liable-Sands, A.L. Rheingold, W. Yao, R.H. Crabtree, New J. Chem. (1998) 1493–1498;
(c) Z. Lu, C.H. Jun, S.R. de Gala, M.P. Sigalas, O. Eisenstein, R.H. Crabtree, Organometallics 14 (1995) 1168–1175;
(d) C.N. Iverson, W.D. Jones, Organometallics 20 (2001) 5745–5750;
(e) X. Zhang, G.B. Carpenter, D.A. Sweigart, Organometallics 18 (1999) 4887–4888.

[4] (a) J.W. Suggs, C.-H. Jun, J. Am. Chem. Soc. 106 (1984) 3054;
(b) J.W. Suggs, C.-H. Jun, J. Am. Chem. Soc. 108 (1986) 4679;
(c) J.W. Suggs, C.-H. Jun, J. Chem. Soc., Chem. Commun. (1985) 92;
(d) N. Chatani, Y. Ie, F. Kakiuchi, S. Murai, J. Am. Chem. Soc. 121 (1999) 8645;
(e) S.-Y. Liou, M.E. van der Boom, D. Milstein, Chem. Commun. (1998) 687;
(f) B. Rybtchinski, S. Oevers, M. Montag, A. Vigalok, H. Rozenberg, J.M.L. Martin, D. Milstein, J. Am. Chem. Soc. 123 (2001) 9064–9077;
(g) A. Sundermann, O. Uzan, D. Milstein, J.M.L. Martin, J. Am. Chem. Soc. 122 (2000) 7095–7104;
(h) B. Rybtchinski, D. Milstein, J. Am. Chem. Soc. 121 (1999) 4528–4529;
(i) C.-H. Jun, C.W. Moon, D.-Y. Lee, Chem. Eur. J. 8 (2002) 2423;
(j) C.-H. Jun, H. Lee, J. Am. Chem. Soc. 121 (1999) 880;
(k) C.-H. Jun, D.-Y. Lee, H. Lee, J.-B. Hong, Angew. Chem. Int. Ed. 39 (2000) 3070;
(l) C.-H. Jun, H. Lee, S.-G. Lim, J. Am. Chem. Soc. 123 (2001) 751.

[5] (a) C.A. Tolman, Chem. Rev. 77 (1977) 313;
(b) R. Mason, D.W. Merck, Angew. Chem. 90 (1978) 195;
(c) P.S. Pregosin, Transition metal nuclear magnetic resonance, Elsevier, Amsterdam, 1991;
(d) C. Brevard, P. Granger, Handbook of High Resolution Multinuclear NMR, Wiley, Chichester, 1981.

[6] G.R. Nuzzo, T.J. McCarthy, G.M. Whitesides, Inorg. Chem. 20 (4) (1981) 1312–1314.

[7] M.J. Frisch, G.W. Trucks, H.B. Schlegel, G.E. Scuseria, M.A. Robb, J.R. Cheeseman, J.A. Montgomery Jr., T. Vreven, K.N. Kudin, J.C. Burant, J.M. Millam, S.S. Iyengar, J. Tomasi, V. Barone, B. Mennucci, M. Cossi, G. Scalmani, N. Rega, G.A. Petersson, H. Nakatsuji, M. Hada, M. Ehara, K. Toyota, R. Fukuda, J. Hasegawa, M. Ishida, T. Nakajima, Y. Honda, O. Kitao, H. Nakai, M. Klene, X. Li, J.E. Knox, H.P. Hratchian, J.B. Cross, C. Adamo, J. Jaramillo, R. Gomperts, R.E. Stratmann, O. Yazyev, A.J. Austin, R. Cammi, C. Pomelli, J.W. Ochterski, P.Y. Ayala, K. Morokuma, G.A. Voth, P. Salvador, J.J. Dannenberg, V.G. Zakrzewski, S. Dapprich, A.D. Daniels, M.C. Strain, O. Farkas, D.K. Malick, A.D. Rabuck, K. Raghavachari, J.B. Foresman, J.V. Ortiz, Q. Cui, A.G. Baboul, S. Clifford, J. Cioslowski, B.B. Stefanov, G. Liu, A. Liashenko, P. Piskorz, I. Komaromi, R.L. Martin, D.J. Fox, T. Keith, M.A. Al-Laham, C.Y. Peng, A. Nanayakkara, M. Challacombe, P.M.W. Gill, B. Johnson, W. Chen, M.W. Wong, C. Gonzalez, J.A. Pople, GAUSSIAN-03, Revision B.01, Gaussian, Inc., Pittsburgh, PA, 2003.

[8] The Basis set was obtained from the Extensible Computational Chemistry Environment Basis Set Database, Version 02/25/04, as developed and distributed by the Molecular Science Computing Facility, Environmental and Molecular Sciences Laboratory which is part of the Pacific Northwest Laboratory, P.O. Box 999, Richland, WA 99352, USA, and funded by the US Department of Energy. The Pacific Northwest Laboratory is a multi-program laboratory operated by Battelle Memorial Institute for the US Department of Energy under Contract DE-AC06-76RLO 1830. Contact David Feller or Karen Schuchardt for further information.

[9] (a) P.-T. Cheng, S.C. Nyburg, Can. J. Chem. 50 (6) (1972) 912–916;
(b) H.C. Clark, G. Ferguson, Mark J. Hampden-Simith, B. Kaitner, H. Ruegger, Polyhedron 7 (1988) 1349–1353.

[10] N.C. Harrison, M. Murray, J.L. Spencer, F.G.A. Stone, J. Chem. Soc., Dalton Trans. (1978) 1337–1342.

[11] (a) G.M. Whitesides, J.F. Gaasch, E.R. Stedronsky, J. Am. Chem. Soc. 94 (1972) 5258–5270;
(b) J. Chatt, R.S. Coffey, A. Gough, D.T. Thompson, J. Chem. Soc. (A) (1968) 190–194;
(c) F. Ozawa, T. Ito, A. Yamamoto, J. Am. Chem. Soc. 102 (1980) 6457–6463.

[12] (a) H. Kwart, J. Slutsky, S.F. Sarner, J. Am. Chem. Soc. 95 (1973) 5242–5244;
(b) P. Krumbiegel, Isotopieeffekte, Akademie-Verlag GmbH, Berlin, 1970.

[13] (a) M. Shampsique, E. Karkhaneei, A. Afkhami, Polyhedron 17 (1998) 3809–3814;
(b) H. Gunther, NMR spectroscopy, Wiley, Chichester, 1995, p. 339;
(c) J.M. Ceraso, P.B. Smith, J.S. Landers, J.L. Dye, J. Phys. Chem. 81 (8) (1977) 760–765.

[14] (a) J.P. Birk, J. Halpern, A.L. Pickard, Inorg. Chem. (1968) 2672–2673;
(b) H.C. Clark, G. Ferguson, Mark J. Hampden-Simith, B. Kaitner, H. Ruegger, Polyhedron 7 (1988) 1349–1353.

[15] K. Ruhland, E. Herdtweck, Adv. Synth. Catal. 347 (2005) 398–404.

[16] A. Gillie, J.K. Stille, J. Am. Chem. Soc. 102 (1980) 4933–4941.

[17] J. Chatt, L.M. Vallarino, L.M. Venanzi, J. Chem. Soc. (1957) 2496–2505.

[18] (a) A.L. van Geet, Anal. Chem. 42 (1970) 679–680;
(b) H. Friebolin, G. Schilling, L. Pohl, Org. Magn. Reson. 12 (1979) 569–573;
(c) C. Piccinni-Leopardii, O. Fabre, J. Reisse, Org. Magn. Reson. 8 (1976) 233–236;

(d) F.H. Köhler, X. Xie, Magn. Reson. Chem. 35 (1997) 487–492.
[19] (a) Data Collection Software for Nonius κ-CCD devices, Delft, The Netherlands, 2001.;
(b) Z. Otwinowski, W. Minor, Methods Enzymol. 276 (1997) 307ff;
(c) A. Altomare, G. Cascarano, C. Giacovazzo, A. Guagliardi, M.C. Burla, G. Polidori, M. Camalli, SIR-92, J. Appl. Crystallogr. 27 (1994) 435–436;
(d) A.J.C. Wilson (Ed.), International Tables for Crystallography, vol. C, Kluwer Academic Publishers, Dordrecht, 1992, Tables 6.1.1.4, 4.2.6.8, and 4.2.4.2;
(e) A.L. Spek, PLATON: A multipurpose crystallographic tool, Utrecht University, Utrecht, The Netherlands, 2001;
(f) G.M. Sheldrick, SHELXL-97, Universität Göttingen, Göttingen, Germany, 1998.